

$$\frac{8}{\pi} \alpha^2 \frac{N}{A} Z^2 r_e^2 \frac{m_e}{m} \approx 10^{-6} \text{ cm}^2 \text{ g}^{-1}.$$

Figure 2 shows the quantity  $UvL(U, v)$  computed for a  $\mu$ -meson of energy  $U = 10^{10}$  ev in lead and plotted against  $v$ . The quantity  $UvL$ , when multiplied by

$$\frac{8}{\pi} \alpha^2 \frac{N}{A} Z^2 r_e^2 \approx 209 \cdot 10^{-6}$$

gives the probability per g  $\text{cm}^{-2}$  and per logarithmic energy interval for the production of a pair of total energy  $Uv$ . For comparison, Fig. 2 also shows the corresponding probabilities for the production of a secondary electron by a collision process and for the production of a secondary photon by a radiation process.

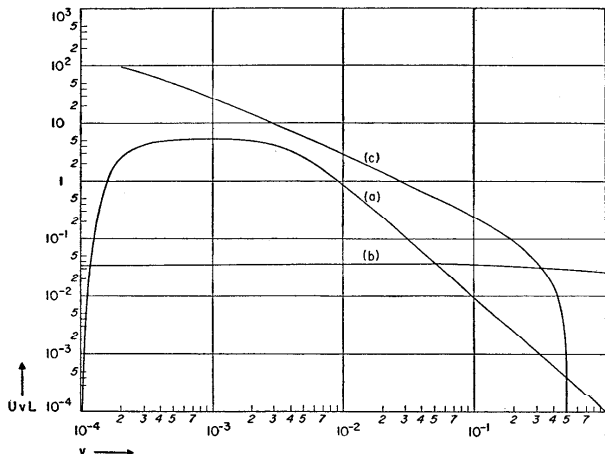


Fig. 2.20.2. Comparison between the differential probabilities of the following processes: (a) direct pair production; (b) radiation; and (c) collision. The curves refer to  $\mu$ -mesons of energy  $U = 10^{10}$  ev, in lead. The abscissa represents the fractional energy  $v = U'/U$  of the pair in case (a), of the secondary photon in case (b), and of the secondary electron in case (c). The ordinate,  $UvL$ , when multiplied by  $(8/\pi)\alpha^2(N/A)Z^2 r_e^2 \approx 209 \cdot 10^{-6}$ , gives the probability for the process in question per g  $\text{cm}^{-2}$  and per logarithmic interval of  $U'$ . Private communication from R. Davison.

## Experimental Methods

**3.1. General remarks.** The operation of the instruments used for the study of high-energy particles rests upon ionization phenomena and other effects of collision processes by charged particles. These instruments, therefore, detect charged particles directly, whereas they detect neutral particles only indirectly, through the intermediary of the secondary charged particles produced in their passage through matter.

Most of the early experimental work on high-energy particles was carried out by means of *ionization chambers, proportional counters, Geiger-Mueller counters, and cloud chambers*. All of these instruments are essentially ionization detectors. Since about 1946, the method of *photographic emulsions* has acquired great importance and, more recently, *scintillation counters* have proven their value. The basic principles of these methods have been known for many years. Both methods, however, had remained in the background until technical developments increased their practical usefulness.

A detailed description of the instruments listed above is beyond the scope of this volume. However, we shall analyze with some care the nature of the phenomena that are detected so that the reader may gain a clear understanding of the operation of the instruments and may be in a position to evaluate critically the experimental data.

### 3.2. The ionization chamber as an integrating instrument.\*

The ionization chamber measures the total number of ion pairs produced in a certain time interval within a certain volume of gas, the *sensitive volume* of the chamber. It consists essentially of two electrodes separated by a gaseous dielectric and kept at different potentials. The electric field between the electrodes causes the ions, which otherwise would move at random through the gas on account of their thermal agitation, to drift along the electric lines of force, the positive ions moving toward the negative electrode and the negative ions toward the positive electrode. In general, the random velocity is larger than the drift velocity; thus some

\* For further information on this subject see, for instance, the volume *Ionization Chambers and Counters*, by B. Rossi and H. Staub, McGraw-Hill Book Co., Inc., New York (1940).

ions may diffuse against the electric field to the electrode of like sign. Also, some of the ions may combine with ions of the opposite sign before they reach the electrode toward which they are moving. Both of these effects decrease with increasing electric field until eventually nearly every ion formed in the gas reaches the electrode of opposite sign. Correspondingly, the ion current increases toward a maximum, or *saturation* value. Fig. 1 shows the variation of ion current with collecting voltage in a typical case. At the "saturation voltage,"  $V_s$ , practically all of the ions formed in the sensitive volume are collected, and therefore a further increase in voltage causes no further increase in current.

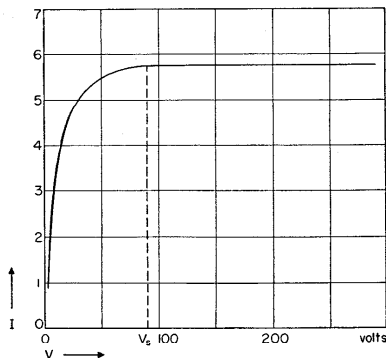


Fig. 3.2.1. Ion current,  $I$  (arbitrary units) vs. collecting voltage,  $V_1$  in a typical ionization chamber.  $V_s$  indicates the saturation voltage.

We shall assume, for the moment, that the rate of ionization does not change with time. The saturation current,  $I$ , is then related to the number,  $N$ , of ion pairs produced per unit time in the sensitive volume of the ion chamber by the equation:

$$I = Ne, \quad (1)$$

where  $e$  is the electron charge.

If the ionization current is sufficiently large it can be measured directly with a moving-coil galvanometer or an electronic galvanometer. Generally, however, it is necessary to use a more sensitive method of detection. This consists of keeping one of the electrodes of the chamber at a constant potential and connecting the other electrode (collecting electrode) to an electrometer. If the difference of potential between the two electrodes is sufficient to insure saturation, the potential,  $V$ , at the collecting electrode changes with time according to the equation:

$$C \frac{dV}{dt} = I = Ne, \quad (2)$$

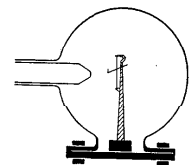
where  $C$  represents the capacity of the collecting electrode and of the electrometer attached to it. One sees that in order to achieve high sensitivity, one must make the capacity  $C$  as small as possible.

In some cases the electrode at constant potential is grounded and the collecting electrode is charged to a potential greater than that necessary for saturation. The collecting electrode is then allowed to discharge, but its voltage is restored to the original value before it drops below the saturation voltage. This method (discharge method) permits the construction of very simple instruments. It has the disadvantage that it does not allow the use of a very sensitive electrometer, since the electrometer is required to stand a voltage greater than the saturation voltage.

In other cases, the collecting electrode is connected periodically to ground and thus kept at a low voltage while the other electrode is held at a constant voltage sufficiently large to insure saturation. In this case one observes the gradual charging up of the collecting electrode in the time interval between two grounding operations. This method (*charge method*) enables one to use more sensitive electrometers. It also permits the use of a *guard electrode* to prevent leakage currents from the high-voltage electrode to the collecting electrode.

A typical ionization chamber of the first type for cosmic-ray research is schematically represented in Fig. 2. The description of this chamber follows, in the words of the authors, Millikan and Neher (MRA36).

"This instrument . . . consisted of a spherical steel bulb of 3-mm wall thickness and 15-cm diameter filled with gas at pressures up to 30 atmospheres and holding at its center a gilded quartz fiber electroscopie system, readable, by means of a short-focus telescope, through a window in the wall. Such an electroscopie with no outside connections of any kind, if properly dried with phosphorous pentoxide, eliminates the serious uncertainties and difficulties inherent in electroscopes having outside connections, especially when these are used in moist surroundings. . . . The design of the suspension of this electroscopie is shown in Fig. 3. The system is of the torsion type and is made entirely of fused quartz. The 5-micron fiber,  $a$ , is stretched until its length is increased about one percent. The 30-micron movable cross arm,  $b$ , is bent at right angles at one end where it is drawn down to a thickness of about 10 microns. The image of  $c$  cast on the recording film by a lens giving a magnification of 10 has then a convenient width on the film. The short bit of fiber  $d$  serves as a fiducial mark and it, together with the part  $e$  (which is bent into the arc of a circle with the torsion fiber as a center) and the stop  $f$ , combine to give a linear scale over practically the whole range of discharge.  $g$  is a piece of platinum cemented to the quartz and is the point at which a new charge is automatically placed on the system at regular time intervals. With a very small oxygen flame all joints are fused



▨ = quartz  
■ = metal

Fig. 3.2.2. Schematic drawing of an ionization chamber used by Millikan *et al.* (MRA36).

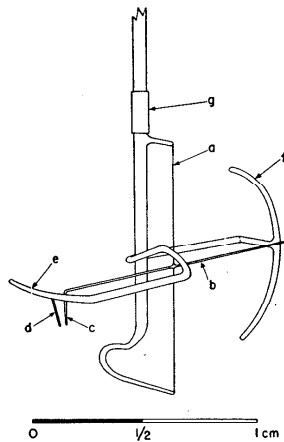


Fig. 3.2.3. Electrometer element of the ionization chamber shown in Fig. 2 (MRA36).

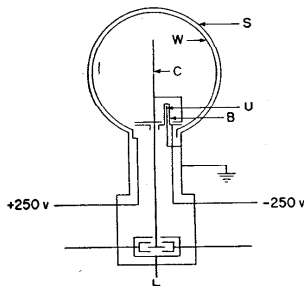


Fig. 3.2.4. Schematic diagram of the Carnegie Model C cosmic-ray ionization chamber used by Compton *et al.* (CAH34). *S*, steel shell; *W*, chamber wall; *C*, collecting electrode; *B*, balance chamber; *U*, uranium source; *L*, Lindemann electrometer.

together so that the whole system becomes essentially one piece of quartz. A twist of about  $30^\circ$  is placed permanently in the torsion fiber so that no motion of the movable arm takes place until about 250 volts are reached and then the full deflection of 2 mm results for the next 75 volts. The whole system from *a* down is covered with a conducting layer of gold by evaporation. The movable part *b* is balanced by cutting off one end until a tilt of  $90^\circ$  causes less than 0.005 mm actual motion of *c*. Besides being free from tilt, the system, because of the large ratio of strength to weight,

is quite insensitive to vibration. The electrostatic capacity is approximately 0.43 cm. In a 100-division scale placed in the eyepiece the voltage sensitivity is about 0.7 volt/div."

An example of an ionization chamber of the second type with the additional feature of a "compensating current" is the Carnegie Model C Cosmic-Ray Meter (CAH34), shown schematically in Fig. 4. The volume of this chamber is 19.3 liters, and it is filled to a pressure of 50 atmospheres with highly purified argon. A Lindemann electrometer is charged by the difference in current arising from the main chamber and a small balance chamber containing a uranium radioactive source. By adjusting the position of the uranium one makes the average current in the balance chamber approximately equal to the average current in the main chamber, so that the electrometer measures essentially deviations from a predetermined mean. Hence the voltage on the electrometer never becomes very large. The balance chamber serves further to cancel the effects of pressure, temperature, and variations of the supply voltage. The integration time of the instrument is usually about one hour, and one terminates this period by grounding the central electrode, *C*. The chamber is operated at a voltage of about 250 volts, which is ample to insure saturation (the saturation curve in Fig. 1 refers to this particular chamber).

An ionization chamber, when used in the manner described at the beginning of this section, measures the integrated effects of a large number of ionizing particles and may therefore be considered as an *integrating* instrument. For its operation it is immaterial whether the electrons formed by the ionizing agent remain free (as they do in argon, for example) or whether they attach themselves to neutral molecules forming heavier, more slowly moving, negative ions (as they do in oxygen). The probability of recombination, however, is increased by attachment, and a higher field strength may be necessary to attain saturation. When the ionization current is measured by means of an electrometer, the "integration time" is the time between successive determinations of the voltage of the collecting electrode. When the ionization current is measured by means of a galvanometer, the integration time is determined essentially by the oscillation period of this instrument.

Successive determinations of the ionization current caused by an ionizing radiation of constant intensity show statistical fluctuations due to the discontinuous character of the ionization process. In relative value, these statistical fluctuations are approximately equal to the statistical fluctuations in the number of ionizing rays traversing the chamber during the integration time and are, therefore, inversely proportional to the square root of this time.

**3.3. The ionization chamber as a pulse instrument.\*** One can use an ionization chamber not only to determine the integrated effects of a large number of ionizing particles, but also to measure the ionization produced by a single particle or by a small group of particles traversing the chamber simultaneously. If the ionization produced by this particle

\* For further information on this subject, the reader may consult an article by Corson and Wilson (CDR48) and the volume *Ionization Chambers and Counters*, by R. Rossi and H. Staub, McGraw-Hill Book Co., Inc. (1949), Chapter III.

or particles is sufficiently large, the voltage pulse that appears at the collecting electrode can be recorded by means of a sensitive electrometer or an electronic pulse amplifier.

The variation of the voltage at the collecting electrode is due to electrostatic induction of the ions moving through the gas. It begins at the moment when the ions are produced and, if the collecting electrode is perfectly insulated, it ends at the moment when all ions have been collected.

The "pulse shape," i.e., the curve representing voltage as a function of time, depends on the drift velocities of the ions. The drift velocities of both heavy ions and free electrons depend on the nature of the gas. The drift velocity of heavy ions is directly proportional to the electric field strength and inversely proportional to the gas pressure. It is of the order of  $1 \text{ cm sec}^{-1}$  at one atmosphere in a field of  $1 \text{ volt cm}^{-1}$ , and of the order of  $10^8$  or  $10^9 \text{ cm sec}^{-1}$  under the ordinary operating conditions of a pulse chamber. The drift velocity of electrons, too, depends on the ratio

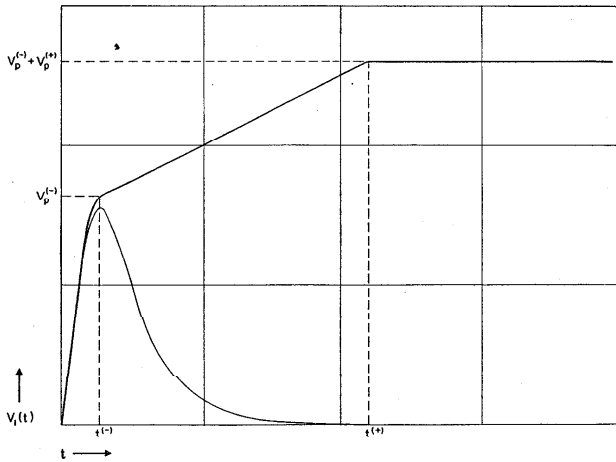


Fig. 3.3.1. Time dependence of the voltage,  $V_1(t)$ , at the collecting electrode of a pulse ionization chamber. The upper curve refers to the case that the collecting electrode is insulated; the lower curve to the case that the collecting electrode is grounded through a resistor.  $t^{(-)}$  and  $t^{(+)}$  represent the collection times of electrons and positive ions respectively.  $V_p^{(-)}$  and  $V_p^{(+)}$  are voltage pulses caused by the motion of electrons and positive ions, respectively. Schematic diagram; the drift velocity of electrons is taken as equal to about ten times that of positive ions to facilitate graphic representation of the pulse.

of electric field strength to pressure, but is not a simple function of this ratio. Under ordinary operating conditions, it is of the order of  $10^8 \text{ cm sec}^{-1}$ .

If the electrons remain free, the pulse consists of two distinct parts, an initial fast rise, caused by the rapid motion of the electrons, which ceases when all the electrons have been collected, followed by a slower rise, caused by the motion of the positive ions. The upper curve of Fig. 1 indicates the nature of the voltage pulse in such cases. If electron attachment takes place, no rapid rise is observed, since the drift velocities of the heavy negative ions formed as a result of electron attachment are of the same order of magnitude as the drift velocities of positive ions.

The rate of change of the voltage of the collecting electrode, at any particular time, depends on the distribution of ions through the chamber and on their drift velocities. One can obtain an expression for this rate of change in a very simple and very general manner by applying the principle of conservation of energy. The only approximation that will be made is the neglect of "edge effects," i.e., of induction phenomena caused by the motion of ions in the neighborhood of the boundary of the sensitive volume. To avoid difficulties in this connection, we shall assume that the high-voltage electrode surrounds the collecting electrode completely, so that the sensitive volume is bounded by the surfaces of the electrodes.

Let  $n^{(+)}$  and  $n^{(-)}$  be the numbers of positive and negative ions per unit volume,  $w^{(+)}$  and  $w^{(-)}$  their drift velocities. The density of space charge,  $\rho$ , in the dielectric has then the expression:

$$\rho = e[n^{(+)} - n^{(-)}] \quad (1)$$

and the density of electric current,  $j$ , is

$$j = e[n^{(+)}w^{(+)} - n^{(-)}w^{(-)}]. \quad (2)$$

The quantities  $\rho$  and  $j$  are related to one another by the well known continuity equation

$$\text{div } j \pm \frac{\partial \rho}{\partial t}. \quad (3)$$

Let the outer electrode (high voltage electrode) be at the constant potential  $V_0$ . Suppose that the inner electrode (collecting electrode) is insulated and let  $V_1(t)$  be its potential at the time  $t$ .

Since the field equations are linear, we may consider the electric field in the dielectric as the superposition of the field caused by the voltage difference between the electrodes when no space charge is present, and the field produced by the space charge, with both electrodes at zero potential. Let  $\mathcal{E}$ ,  $\mathcal{E}_p$  represent the field intensities and  $V$ ,  $V_p$  the scalar potentials of the two fields. These quantities satisfy the following equations:

$$\begin{aligned} \text{div } \mathcal{E} &= 0, & \text{div } \mathcal{E}_p &= 4\pi\rho; \\ \mathcal{E} &= -\text{grad } V, & \mathcal{E}_p &= -\text{grad } V_p; \end{aligned} \quad (4)$$

and the following boundary conditions:

$$\begin{aligned} \text{at the high-voltage electrode: } & V = V_0, \quad V_p = 0; \\ \text{at the collecting electrode: } & V = V_1(t), \quad V_p = 0. \end{aligned} \quad (5)$$

In order to write the energy equation, consider that ions and electrons move with approximately constant average speed through the gas. Therefore the amount of energy that they deliver to the gas in the form of heat equals the work performed upon them by the electric field. This quantity, in turn, must equal the decrease in the electrostatic energy of the field. Thus we arrive at the following equation:

$$-\frac{d}{dt} \int_v \frac{(\mathcal{E} + \mathcal{E}_p)^2}{8\pi} dv = e \int_v (\mathcal{E} + \mathcal{E}_p) [n^{(+)} \mathbf{w}^{(+)} - n^{(-)} \mathbf{w}^{(-)}] dv, \quad (6)$$

where both integrals extend over the sensitive volume,  $v$ , of the chamber.

The identity for the divergence of the product of a scalar and a vector yields:

$$\int_v \mathcal{E} \cdot \mathcal{E}_p dv = \int_v V_p \operatorname{div} \mathcal{E} dv - \int_v \operatorname{div} (V_p \mathcal{E}) dv. \quad (7)$$

The first term on the right side is zero on account of (4). Application of the divergence theorem to the second term gives:

$$\int_v \operatorname{div} (V_p \mathcal{E}) dv = \int_s V_p \mathcal{E}_n ds,$$

where  $s$  is the boundary of the sensitive volume (which, according to our assumption, consists of the combined surface of the two electrodes) and  $\mathcal{E}_n$  is the component of  $\mathcal{E}$  perpendicular to this surface ( $\mathcal{E}_n = |\mathcal{E}|$ ). The integral on the right hand side is zero because of the boundary condition for  $V_p$ ; therefore:

$$\int_v \mathcal{E} \cdot \mathcal{E}_p dv = 0. \quad (8)$$

Eqs. (3) and (4) yield:

$$\frac{1}{4\pi} \operatorname{div} \frac{\partial \mathcal{E}_p}{\partial t} = -\operatorname{div} j. \quad (9)$$

If we multiply both sides of Eq. (9) by  $V_p$ , apply the identity for the divergence of a product, integrate over the sensitive volume and consider the boundary condition on  $V_p$ , we obtain the following identity:

$$\frac{1}{4\pi} \int_v \mathcal{E}_p \frac{\partial \mathcal{E}_p}{\partial t} dv = -e \int_v \mathcal{E}_p [n^{(+)} \mathbf{w}^{(+)} - n^{(-)} \mathbf{w}^{(-)}] dv. \quad (10)$$

On the other hand, the energy of the field produced by the voltage difference between the two electrodes is just the energy of a charged condenser. If we call  $C$  the capacity of this condenser, we can write the following identity:

$$\int_v \frac{\mathcal{E}^2}{8\pi} dv = \frac{1}{2} C (V_0 - V_1)^2. \quad (11)$$

By combining Eqs. (6), (8), (10) and (11) we obtain the desired expression for  $dV_1/dt$  in terms of the densities of positive and negative ions,  $n^{(+)}$  and  $n^{(-)}$ , and of their drift velocities,  $\mathbf{w}^{(+)}$  and  $\mathbf{w}^{(-)}$ :

$$C \frac{dV_1}{dt} = \frac{e}{V_0 - V_1} \int_v \mathcal{E} \cdot [n^{(+)} \mathbf{w}^{(+)} - n^{(-)} \mathbf{w}^{(-)}] dv. \quad (12)$$

This is the fundamental equation of the pulse ionization chamber. If we replace the integral by a summation over the individual charges, we may write it as follows:

$$C \frac{dV_1}{dt} = \frac{e}{V_0 - V_1} \sum_i [\mathcal{E}_i^{(+)} \cdot \mathbf{w}_i^{(+)} - \mathcal{E}_i^{(-)} \cdot \mathbf{w}_i^{(-)}], \quad (13)$$

where  $\mathcal{E}_i^{(+)}$  is the electric field intensity at the point where the  $i$ th positive ion finds itself at the time  $t$ ,  $\mathbf{w}_i^{(+)}$  is the drift velocity of this ion, and  $\mathcal{E}_i^{(-)}$ ,  $\mathbf{w}_i^{(-)}$  are the corresponding quantities relative to the  $i$ th negative ion.

Note that the vector  $\mathcal{E}/(V_0 - V_1)$  depends only on the geometry of the chamber (i.e., it is independent of the voltage difference between the electrodes and of the space charge). For example, in the case of a parallel-plate chamber, this vector is perpendicular to the plates and its magnitude is the inverse distance between the plates.

The form of Eqs. (12) and (13) shows that one may consider the observed pulse as the superposition of two pulses, one due to the motion of the positive ions, the other due to the motion of the negative ions. Assume  $V_1 = 0$  at  $t = 0$ , i.e., at the time when the ionizing particle passes through the chamber. Integration of Eq. (13) yields:

$$V(t) = V_1^{(+)}(t) + V_1^{(-)}(t), \quad (14)$$

where

$$CV_1^{(+)}(t) = \int_0^t \frac{e}{V_0 - V_1} \sum_i \mathcal{E}_i^{(+)} \cdot \mathbf{w}_i^{(+)} dt', \quad (15)$$

$$CV_1^{(-)}(t) = - \int_0^t \frac{e}{V_0 - V_1} \sum_i \mathcal{E}_i^{(-)} \cdot \mathbf{w}_i^{(-)} dt'.$$

Note that  $\mathbf{w}_i^{(+)} dt'$  [or  $\mathbf{w}_i^{(-)} dt'$ ] is the infinitesimal displacement of the  $i$ th positive (or negative) ion in the time  $dt'$ . Note also that, since the ratio  $\mathcal{E}/(V_0 - V_1)$  remains constant, one can replace it by the ratio  $\mathcal{E}_0/V_0$  where  $\mathcal{E}_0$  is the field intensity at  $t = 0$ . Equations (15) then yield:

$$CV_1^{(+)}(t) = \frac{e}{V_0} \sum_i (V_i^{(+)}(0) - V_i^{(+)}(t)), \quad (16)$$

$$CV_1^{(-)}(t) = - \frac{e}{V_0} \sum_i (V_i^{(-)}(0) - V_i^{(-)}(t)),$$

where  $V_i^{(+)}(t)$  [or  $V_i^{(-)}(t)$ ] is the voltage at the position occupied by the  $i$ th positive (or negative) ion at the time  $t$ , computed as if  $V_1$  were zero and if no space charge were present.  $V_i^{(+)}(0)$  and  $V_i^{(-)}(0)$  are both equal to the voltage at the place where the  $i$ th ion pair is produced and can be denoted by a common symbol,  $V_i(0)$ .

Suppose, for example, that the high-voltage electrode is positive with respect to the collecting electrode. Then, if  $t$  is larger than the collection time of positive ions,  $V_i^{(+)}(t) = 0$ . Similarly, if  $t$  is larger than the collection time of negative ions,  $V_i^{(-)}(t) = V_0$ . The total voltage pulses,  $V_p^{(+)}$  and  $V_p^{(-)}$ , produced by the motion of positive and negative ions respectively are thus given by the equations:

$$CV_p^{(+)} = \frac{e}{V_0} \sum_i V_i(0)$$

$$CV_p^{(-)} = \frac{e}{V_0} \sum_i (V_0 - V_i(0)). \quad (17)$$

If  $N$  is the total number of ion pairs, one obtains from Eqs. (17) the following obvious result for the voltage pulse,  $V_p$ , produced by the motion of ions of both signs:

$$CV_p = Ne. \quad (18)$$

As pointed out previously, if the electrons remain free the pulse due to the motion of the electrons is completed practically before the pulse due to the motion of the positive ions has begun. There are electronic devices that respond to the initial fast rise of the voltage pulse but not to the following slow rise, and thus record only the pulse due to the motion of the electrons. The simplest of such devices is shown in Fig. 2. The collecting electrode is connected to the input of an electronic amplifier and, at the same time, is grounded through a resistor  $R$ . Let  $C$  be the capacity of the collecting electrode, including that of all conductors con-

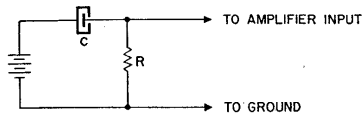


Fig. 3.3.2. Electric connections of a pulse ionization chamber.

nected with it. Suppose that the product  $RC$ , that represents the time constant of the collecting electrode, is large compared with the collection time of electrons, but small compared with the collection time of positive ions. The collecting electrode will then react to the fast electron pulse approximately as if it were electrically insulated, whereas it will react to the slow ion pulse approximately as if it were directly grounded. The actual time-dependence of the voltage will be of the type schematically represented by the lower curve in Fig. 1. One sees that the maximum value of the voltage is practically equal to the voltage pulse,  $V_p^{(-)}$ , caused by the motion of the electrons, as given by the second of Eqs. (17).

The fractional magnitude of the electron pulse, i.e., the quantity

$$V_p^{(-)} / [V_p^{(+)} + V_p^{(-)}] = eV_p^{(-)} / Ne$$

depends on the geometry of the ionization chamber and on the place in the chamber where the ionization occurs.

For example, in a chamber with plane and parallel electrodes the field is uniform. In this case [see Eqs. (17)] the electron pulse is to the total pulse as the average distance of the initial ionization from the positive electrode is to the separation of the two electrodes.

Consider, instead, an ionization chamber with cylindrical or spherical geometry and assume that the diameter of the inner electrode (collecting electrode) is small compared with that of the outer electrode (high-voltage electrode). In this case most of the voltage drop occurs near the inner electrode. Therefore, if the inner electrode is positive, the electron pulse will always be close to the total pulse, unless the initial ionization happens to occur in the immediate vicinity of the inner electrode. For this reason a cylindrical or spherical geometry is often preferred to a plane geometry in the design of pulse ionization chambers.

A typical pulse ionization chamber used by Bridge, Hazen, Rossi, and Williams (BHS48.2) is shown in Fig. 3. In the words of these authors: "... The outer shell  $H$ , which is also the high-voltage electrode, consists of a brass tube 3 inches in outer diameter with  $\frac{1}{8}$ -inch walls. The collecting electrode,  $C$ , is a kovar wire, 0.025 inch in diameter and  $20\frac{1}{8}$  inch effective length stretched along the axis of the brass tube. This wire is supported by the glass-kovar seals shown in the figure. The kovar cylinders,  $G$ ,

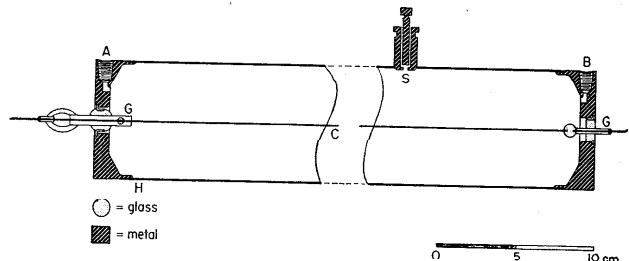


Fig. 3.3.3. Schematic diagram of a pulse ionization chamber.  $H$ , high voltage electrode;  $C$ , central electrode;  $G$ , guard electrodes;  $A$ ,  $B$ , gas inlets;  $S$ , calibration source. From Bridge *et al.* (BHS48.2).

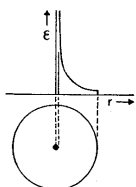
(guard electrodes) are grounded during operation to prevent leakage of charges from the high-voltage electrode to the collecting electrode.  $S$  represents a polonium source, which is used for the calibration of the chamber. . . . The chamber is filled to a pressure of 5 atmospheres with purified argon. The outer shell is kept at a fixed negative voltage  $V_0$  of about 1500 volts. The electron collection time is about 7 micro-

seconds. A polonium alpha particle losing all of its energy (5.3 Mev) within the sensitive volume of the chamber produces an electron pulse of about 5 millivolts.

**3.4. Proportional counters.\*** The pulse produced in an ionization chamber by a single particle of low specific ionization (high-velocity, singly charged particle) is often so small that it cannot be conveniently detected electronically because of the limitations imposed by tube noise. In order to increase the size of the electrical pulse to be detected, one may take advantage of *gas multiplication*.

The chambers designed for use with gas multiplication are generally cylindrical in shape with the collecting electrode in the form of a thin wire stretched along the axis of the tube. Assume that the chamber is filled with a gas in which electron attachment does not take place and that the wire is positive with respect to the outer cylinder. The distribution of field is shown in Fig. 1. If the field near the wire is strong enough,

Fig. 3.4.1. Electric field in a cylindrical counter.



the electrons in that region can acquire sufficient energy between collisions to *ionize* the gas molecules with which they collide. Electrons, produced anywhere in the gas, drift toward the wire; as soon as they enter the multiplication region, they produce secondary electrons by collision. These, in turn, produce more electrons, so that eventually for every electron produced directly by the ionizing agent, an avalanche of  $n$  electrons will reach the collecting electrode. If one increases the voltage across the chamber, the boundary of the multiplication region moves outward, and the size of the avalanche increases.

If ionization by collision were the only phenomenon to be considered, the avalanche would terminate because electrons of successive generations are produced closer and closer to the wire and therefore have less and less chance of multiplying further. However, the multiplication process is complicated by the presence of photons, whose emission always accompanies ionization by collision. Some of these photons release more electrons from the walls of the tube or from the gas by photoelectric

\* For further information on this subject, consult the volumes: *Electrons and Nuclear Counters*, by S. A. Korff, D. Van Nostrand Co., Inc., New York (1946), Chapter 3; and *Ionization Chambers and Counters* by B. Rossi and H. Staub, McGraw-Hill Book Co., Inc., New York (1949), Chapter 4. Consult also (CDR48).

effect. The number of photoelectrons is proportional to the number,  $n$ , of electrons in the first avalanche; let  $\gamma$  be the constant of proportionality. Each of these photoelectrons will multiply by collision, producing a second avalanche of  $\gamma n^2$  electrons, and so on. The total number of electrons reaching the wire for every electron initially formed in the gas is given by the infinite series:

$$n + \gamma n^2 + \gamma^2 n^3 + \dots \quad (1)$$

Clearly,  $n$  increases with voltage. If the voltage is sufficiently small so that  $\gamma n < 1$ , the series (1) converges to the following value:

$$M = \frac{n}{1 - \gamma n} \quad (2)$$

This means that the total number of electrons that arrive at the wire is *proportional* to the initial ionization. The proportionality factor,  $M$ , is called the *multiplication factor*, and a chamber operated under these conditions is called a *proportional counter*.

The voltage pulse at the wire of a proportional counter is qualitatively illustrated in Fig. 2 (heavy line). First, there is a small, usually undetectable voltage rise (from 0 to  $t_1$ ) caused by the motion of the initial electrons to the boundary of the multiplication region. Next comes a very fast rise (from  $t_1$  to  $t_2$ ) as the electrons multiply and drift toward the wire. Last comes the pulse caused by the outward motion of the positive ions (from  $t_2$  to  $t_3$ ). This represents the main part of the pulse. In fact, ac-

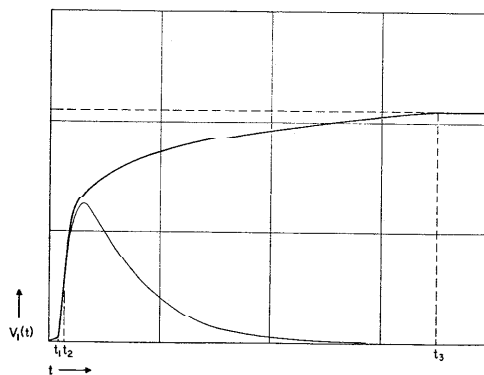


Fig. 3.4.2. Shape of the pulse from a proportional counter (schematic). The heavy line refers to the case that the collecting electrode is insulated; the thin line to the case that the collecting electrode is grounded through a resistor.

ording to Eqs. (3.3.17) the pulses due to the negative and positive partners of an ion pair produced a distance  $r$  from the axis of the wire are in the ratio  $\ln(r/a)/\ln(b/r)$ , where  $a$  and  $b$  are the radii of the wire and of the outer cylinder respectively. Since the gas multiplication occurs in the immediate neighborhood of the wire, this ratio is usually less than one.

The ion pulse rises quite fast at the beginning and then much more slowly as the ions move into regions of weaker field. One can easily see that the rate of change of the voltage at a given time is inversely proportional to the square of the distance,  $r$ , of the positive ion sheath from the axis of the counters. This follows immediately from Eq. (3.3.12) if one remembers that the drift velocity of positive ions is directly proportional to  $E$  and that  $E$ , in a cylindrical counter, is proportional to  $1/r$ . Thus the voltage reaches a large fraction of its final value in a time short compared with the collection time of the positive ions.

The following is actual time scale of events in a typical proportional counter (wire diameter: of the order of 0.01 cm; cylinder diameter of the order of several centimeters). "Waiting time" (from 0 to  $t_1$  in Fig. 2), of the order of  $10^{-7}$  seconds;  $\frac{1}{10}$  of the final pulse height reached in a time of the order of several  $10^{-7}$  seconds;  $\frac{1}{2}$  of the final pulse height reached in a time of the order of several  $10^{-6}$  seconds; collection of positive ions completed at a time of the order of  $10^{-3}$  seconds.

Proportional counters can be used with multiplication factors up to several thousand. However, it is advisable not to exceed a value of about 100 unless the primary ionization is very small. For larger multiplication factors, the counter may become unstable; also the large space charge developed around the wire may destroy the proportionality of its response.

The pulses of proportional counters are usually recorded electronically. The connection to the amplifier input is generally of the type shown in Fig. 3.3.2, with the leak resistor adjusted to give a time constant of the order of  $10^{-6}$  to  $10^{-5}$  seconds. The pulse shape is then of the type shown by the thin line in Fig. 2. The maximum value that the voltage of the wire reaches under these conditions is much smaller than the full pulse height. However, it is a practically constant fraction of it because all pulses of a proportional counter have approximately the same shape.

Proportional counters have been used over a wide range of pressures and physical sizes. V. Cocconi-Tongiorgi (CV49), for example, described a counter used for the detection of cosmic-ray neutrons near thermal energies that is similar in construction to the pulse-type ionization chamber shown in Fig. 3.3.3. The diameter of the wire is 0.01 cm and that of the tube is 2.5 cm. The counter is filled to a total pressure of about 1.8 atmospheres, 1.5 atmosphere being  $B^{10}$ -enriched  $BF_3$  and 0.3 atmosphere being argon. Thermal neutrons in crossing such a counter along a diameter have a probability of about 0.3 of reacting with a boron nucleus so as to initiate the reaction  $B^{10} + n \rightarrow He^4 + Li^7$ . The output pulse from the counter is then proportional to the amount of ionization produced in the gas by the  $He^4$  and  $Li^7$  ions.

The gas pressure in the counter described above is higher than in most proportional

counters. This requires higher voltage and greater purity of the gas. On the other hand, the higher pressure results in greater efficiency for the detection of neutrons, and in more uniform pulses.

**3.5. Geiger-Mueller tubes.\*** Consider a counter tube of the type described in the previous section and suppose that the potential difference between the cylinder and the wire is gradually increased until the number of photo-electrons from the photons produced in the first avalanche becomes greater than the original number of electrons ( $\gamma n > 1$ ). In this case the series (3.4.1), giving the total number of electrons produced per primary ion pair, diverges. Physically this means that a discharge takes place. If the potential difference is not too far above threshold (i.e., if  $\gamma n$  is not much larger than 1) the discharge may not be self-sustaining. Thus the counter can record individually each ionizing particle that passes through it.

A counter operated under these conditions is called a discharge counter, or more specifically (when it is of cylindrical shape) a Geiger-Mueller counter or Geiger-Mueller tube (GH28). Such a counter has two salient features. First, the pulses are usually several volts in size and therefore can be detected without any further electronic amplification. Second, the size of the pulses is not proportional to the initial ionization, but is determined by the characteristics of the counter and by the conditions under which it operates.

Discharge counters fall into two categories, depending on whether they are filled with a simple gas (hydrogen, argon, air, etc.) or with a mixture of a simple gas and a complex polyatomic gas (alcohol, ether, etc.). Polyatomic-gas counters were first used by Trost (TA37). We shall discuss separately the various phases of the discharge for counters of the two different types.

**A. The Initial Avalanche.** The multiplication by collision of the electrons produced by the primary ionizing agent takes place in exactly the same manner in the discharge counters of the two types mentioned above as in the proportional counters. It is characterized by the multiplication factor,  $n$ , in the first avalanche.

**B. The Spreading of the Discharge.** The discharge spreads through the counter by virtue of the photoelectric effect.

Photoelectric effect plays a relatively minor role in the proportional counter ( $\gamma n \ll 1$ ). Therefore, in a proportional counter the secondary ionization is essentially confined to the section of the tube where the initial ionization occurs.

In a discharge counter with a simple-gas filling, the photons emitted by the excited atoms travel toward the cathode to release photoelectrons

\* For a more complete discussion of the operation of Geiger-Mueller tubes, consult reference (BSC48).



which then undergo further multiplication. Thus, the discharge spreads throughout the whole counter almost instantaneously.

In a discharge counter with a polyatomic-gas mixture (for instance, argon and alcohol) the photons emitted by the atoms of the simple gas (argon) are readily absorbed by the complex molecules (alcohol) and cause them to become ionized. In this case the propagation of the discharge is due to photoelectric effect on the complex molecules of the gas, rather than on the metal of the cathode. Since the mean free path of photons before absorption is very small, the photons remain confined to a thin sheath around the wire and the discharge propagates along the wire with moderate velocity (from 2 to 20 centimeters per microsecond depending on the counter filling and operating voltage). The correctness of this view is proved by the fact that a small glass bead on the wire is sufficient to stop the propagation of the discharge (SHG42).

**C. The Quenching of the Discharge.** In both types of discharge counters, as the ions multiply, a dense sheath of positive ions forms around the wire. This positive-ion sheath effectively increases the diameter of the anode and therefore decreases the field intensity around it. Eventually the maximum field intensity drops below the value necessary for supporting further ionization. In the region where this happens, the discharge ceases. Notice that when the gas filling contains an organic vapor the discharge in one section of the counter may cease while in another section it has not yet begun.

**D. After Discharges.** The positive ions start moving outward toward the cathode. Consider first the case of the simple-gas counter, for instance, an argon counter. When the argon ions arrive in the vicinity of the cathode, they draw electrons out of the cathode and combine with them to become neutral atoms. However, the ionization energy of argon is much greater than the work function of the metal (i.e., the energy required to extract an electron from the metal). The excess energy is released in the form of a photon which, in turn, may release a second electron from the metal and thus initiate a second discharge.

Therefore, in a simple-gas counter the discharge, originally quenched by the positive-ion sheath growing around the wire, will start again as soon as the ion sheath reaches the cathode. One must, of course, prevent the rekindling of the discharge if one wants to use the counter to record individual ionizing particles. One can accomplish this purpose by means of an electronic circuit that lowers the voltage difference between the wire and the cylinder for a sufficient length of time after each discharge. More simply, one can connect the wire to ground through a very large resistor (of the order of 1000 megohms), which allows the voltage of the wire to drop until the difference of voltage between wire and cathode is no longer sufficient to sustain the discharge.

Consider next the case of a polyatomic-gas counter (for instance, an argon-alcohol counter). A positive argon ion cannot reach the cathode without undergoing a large number of collisions with alcohol molecules. Since the ionization potential of the argon atom is greater than the ionization potential of the alcohol molecule, a transfer of charge will eventually occur from argon ions to alcohol molecules, so that all argon ions become neutralized and only alcohol ions reach the cathode. At the cathode the ionized alcohol molecules will become neutral molecules by extracting electrons from the cathode.

As in the case of the argon ions, the ionization potential is much greater than the work function so that the alcohol molecule is left in an excited state. However, instead of releasing the excitation energy in the form of a photon, the alcohol molecule will *dissociate*. Since no secondary photons are emitted at the arrival of the positive ions at the cathode, there will be no occasion for the discharge to start again. Thus, polyatomic-gas counters do not require an external quenching device, and for this reason are often called *self-quenching* counters. This designation is perhaps somewhat misleading because in both types of counters the discharge is quenched by the building up of the space charge around the wire. The only difference is that in the simple-gas counter a secondary discharge begins when the positive ions reach the cathode, whereas in the polyatomic-gas counter this does not happen.

**3.6. Operation characteristics of Geiger-Mueller counters.** Figure 1 shows the construction of a Geiger-Mueller counter of the type used for cosmic-ray experiments. The dimensions of Geiger-Mueller count-

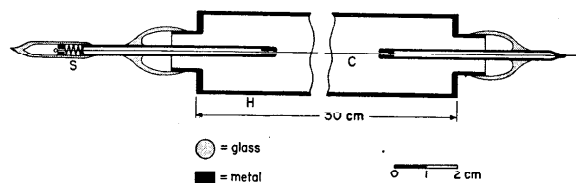


Fig. 3.6.1. Construction of a typical Geiger-Mueller tube. H, high-voltage electrode (brass); C, central electrode (5 mil tungsten wire); S, spring (to hold wire in tension).

ers vary over a wide range—from a few millimeters to about 10 centimeters for the diameter and from about one centimeter to about one meter for the length. The gas pressure is usually of the order of 10 centimeters of mercury. In the self-quenching counters the partial pressure of the polyatomic gas is about one-tenth of that of the simple gas.

Figure 2 shows the characteristic dependence of counting rate on voltage between the electrodes for a Geiger-Mueller counter of the type shown in Fig. 1, exposed to a source of radiation of constant intensity. The lowest voltage at which counts are recorded is called the "threshold" voltage. Its value depends to a small extent on the minimum pulse height required to operate the recording instrument. When the voltage is raised above the threshold, the counting rate increases rapidly and soon reaches a saturation value, after which it remains almost constant for a further increase of the voltage of the order of several hundred volts. Eventually, however, the counting rate begins to increase again more and more rapidly until a continuous discharge sets in.

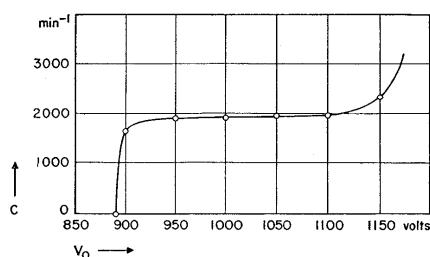


Fig. 3.6.2. Dependence of the counting rate,  $C$ , on the voltage,  $V_0$ , in a Geiger-Mueller tube.

The flat portion of the curve representing the counting rate as a function of voltage is called the "plateau." In this region the counter records practically all of the ionizing particles that traverse its sensitive volume (see below). However, the counting rate on the plateau is not completely independent of voltage. In a "good" counter the counting rate increases by several per cent from one end of the plateau to the other. In a "poor" counter the increase is greater. This increase is caused by secondary discharges whose number increases with increasing voltage and which are probably due to the formation of metastable molecules that release electrons in colliding with the counter walls.

In a self-quenching counter the size of the pulse is directly proportional to the length of the wire and inversely proportional to the total capacity of the wire and of the conductors connected with it. This is so because the quenching of the discharge requires an ion sheath of a given density to be formed around the wire. Therefore, the discharge is quenched after a given charge per unit length of the wire has been produced in the counter.

The pulse of the Geiger-Mueller counter starts with a small variable delay (spontaneous time lag) after the traversal of the ionizing particle.

This delay represents the time needed by the electrons to travel from the place where they are produced to the neighborhood of the central wire where gas multiplication begins. It corresponds to the "waiting time" of the proportional counters and it is of the order of several tenths of a microsecond. The pulse, which is due to the outward motion of the positive-ion sheath, rises very rapidly at first and then more slowly. The speed of the initial rise depends to a large extent on the velocity of propagation of the discharge through the counter and is of the order of ten volts per microsecond. Once the discharge has spread through the whole counter, the rate of the voltage rise is determined by the drift velocity of the positive ions.

As the positive ions move outward, the electric field strength in the vicinity of the wire increases and eventually reaches the minimum value necessary for a new discharge to take place. Until this happens the counter is completely insensitive. Once the field has recovered to the threshold value, the counter is again in a position to record pulses. The size of these pulses increases from zero to the normal value as the continued outward motion of the positive ions restores the field to its original strength. The time during which the counter is completely insensitive is usually called the *dead time*. The time during which it records pulses of reduced size is called the *recovery time*. Both times are of the order of  $2 \cdot 10^{-4}$  sec.

Another quantity of practical importance is the time  $\tau$  after which the size of the pulses is sufficiently large to be recorded by the specific recording instrument used. One can easily see that if  $C$  is the number of ionizing particles per second traversing the counter, the fractional number of pulses that are missed because they follow another pulse with a time separation smaller than  $\tau$  is  $1 - \exp(-C\tau)$ . This quantity may be called the *fractional counting loss*.

**3.7. Coincidence experiments:** Geiger-Mueller counters are often used in groups, and events are detected wherein several counters are discharged simultaneously. These events are called *coincidences*. An ionizing particle capable of traversing several counter walls can produce a coincidence in an array of counters arranged on a straight line. A group of ionizing particles arising from a single secondary interaction can produce a coincidence in an array of counters placed out of line.

Coincidences are usually selected by means of electronic circuits, the prototype of which is shown in Fig. 1 (RB30). The wire of each Geiger-Mueller counter is connected to the grid of a separate vacuum tube. The plates of all the tubes are connected to the positive voltage supply through a common resistor,  $R$ . The value of  $R$  is chosen so that the voltage drop across this resistor is large compared with the voltage drop across the tubes. When a Geiger-Mueller counter is discharged, the grid of the corresponding vacuum tube is driven negative and the plate current is interrupted. If all counters are discharged simultaneously, a large pulse

appears at the common plate lead. If, however, one or more of the counters fail to be discharged, some of the vacuum tubes remain conducting and the output pulse is small.

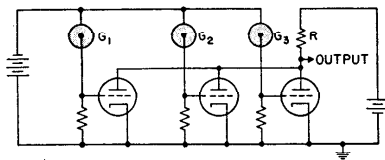


Fig. 3.7.1. Threefold coincidence circuit.  $G_1$ ,  $G_2$ , and  $G_3$  represent three Geiger-Mueller tubes.

An electronically driven mechanical register or another equivalent device records the large output pulses that occur in the event of a coincidence.

In coincidence experiments one must consider the possibility that independent pulses of the different counters, occurring by chance within a very short time interval, may be recorded as simultaneous by the coincidence circuit. The probability of such an event, called a *chance coincidence*, depends on the resolving time of the circuit. Consider, in particular, the case of a twofold coincidence experiment. Define a quantity  $\tau_1$ , such that a pulse of counter 2 appears to be simultaneous with a pulse of counter 1 if it occurs within a time interval  $\tau_1$  from the latter. Define a similar quantity  $\tau_2$  relative to pulses of counter 1 following pulses of counter 2. Let  $C_1$  and  $C_2$  be the counting rates of the two counters (numbers of pulses per unit time). One can compute the number of chance coincidences in the following manner. Suppose that a pulse of counter 1 occurs at the time  $t$ . Clearly a chance coincidence will take place if a pulse of counter 2 occurs at any time in the interval from  $t - \tau_2$  to  $t + \tau_1$ . The length of this time interval is  $\tau_1 + \tau_2$ . If the pulses of counters 1 and 2 are unrelated, the probability for counter 2 to give a pulse in this time interval is  $C_2(\tau_1 + \tau_2)$ . This quantity times the number of pulses per unit time in counter 1 gives the average number,  $\nu$ , of chance coincidences per unit time:

$$\nu = (\tau_1 + \tau_2)C_1C_2. \quad (1)$$

For a coincidence circuit of the type shown in Fig. 1,  $\tau_1$  and  $\tau_2$  represent approximately the times that the vacuum tubes remain nonconducting after each pulse of the corresponding Geiger-Mueller counter. However,  $\tau_1$  and  $\tau_2$  are somewhat shorter than these times because both tubes must be simultaneously nonconducting for a certain minimum time interval before the output voltage reaches the value necessary to operate the recording device. Often  $\tau_1$  and  $\tau_2$  are equal; their common value then defines the *resolving time* of the coincidence circuit. With modern techniques,

one can readily attain resolving times of the order of  $10^{-8}$  sec. However, the variable spontaneous delays of Geiger-Mueller counters usually prevent the use of resolving times shorter than about  $10^{-6}$  sec.

An important question that always arises in the evaluation of counting experiments concerns the statistical fluctuations caused by the random distribution in time of the events recorded. A discussion of this question will be found in Appendix 3.

**3.8. Efficiency of Geiger-Mueller counters.** Except for the counting loss discussed in § 3.6, a Geiger-Mueller counter gives a discharge whenever an ion pair is produced within its sensitive volume. Thus, if the counting rate is not too large, the *efficiency* of a Geiger-Mueller counter, defined as the probability of detecting a particle traversing its sensitive volume, is equal to the probability that the particle produces at least one ion pair within this volume.

This probability is clearly related to the *primary specific ionization* of the particle. Assume, for the moment, that all particles have the same path length of  $l$  centimeters within the sensitive volume. The average number of ionizing collisions in the sensitive volume is then  $j_p \rho l$ , where  $j_p$  is the primary specific ionization (§ 2.10) and  $\rho$  the density of the gas. Let  $w(x)$  be the probability that the particle traverses a thickness of  $x$  gm $^{-2}$  of the gas without undergoing any ionizing collision. The function  $w(x)$  satisfies the differential equation:

$$\frac{dw}{dx} = -wj_p. \quad (2)$$

One can prove this equation easily by considering that  $w(x + dx)$  equals the probability,  $w(x)$ , that the particle goes a distance  $x$  without collisions, times the probability,  $(1 - j_p dx)$ , that no collision occurs in the additional distance  $dx$ . Integration of Eq. (2) with the boundary condition  $w(0) = 1$  yields:

$$w(x) = e^{-j_p x}. \quad (3)$$

The efficiency of the Geiger-Mueller counter,  $\epsilon$ , is then given by the equation:

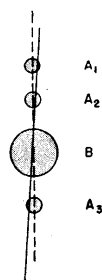
$$\epsilon = 1 - w(\rho l) = 1 - e^{-j_p \rho l}. \quad (4)$$

In practice, there often is a continuous distribution of path lengths. In order to compute the efficiency one must then average the value of  $\epsilon$  given by Eq. (4) over the path-length distribution of the particles under consideration. In this case the efficiency has a complicated expression, but it is still a function of the product  $j_p \rho$ .

\* Equation (4) disregards secondary electrons produced in the counter walls by the incident particle. The increase in efficiency due to these electrons is appreciable when  $\epsilon \ll 1$ .

One can determine experimentally the efficiency of Geiger-Mueller counters for cosmic-ray particles with a method suggested originally by Rossi (RB32.3). Several counters  $A_1, A_2, A_3$  (see Fig. 1) are arranged vertically one above the other to form a "cosmic-ray telescope." The counter under investigation,  $B$ , is placed between the counters of the telescope and one records simultaneously coincidences  $(A_1A_2A_3)$  and  $(A_1A_2A_3B)$ . Since practically all of the coincidences in the cosmic-ray telescope are caused by ionizing particles passing through the counters, the ratio of the  $(A_1A_2A_3B)$  to the  $(A_1A_2A_3)$  coincidence rate represents the efficiency of counter  $B$ . If the dimensions of counters  $A_1, A_2, A_3$  are small compared with those of counter  $B$ , one can investigate the dependence of the efficiency on position by displacing counter  $B$  with respect

Fig. 3.8.1. Experimental arrangement for determining the efficiency of a Geiger-Mueller counter.



to the axis of the telescope. Greisen and Nereson (GKI42), among others, applied this method to a systematic investigation of Geiger-Mueller counters used for cosmic-ray research. They operated with counters 4.24 cm in diameter filled with 10 cm Hg of argon and 1 cm Hg of alcohol vapor, and they found that, at a sufficiently large distance from the ends of the wire, the efficiency is practically 100 per cent throughout the volume of the counter. They also found that the behavior of the efficiency near the ends of the wire depends on the construction of the counter and, more specifically, on the manner in which the wire is supported. In the counters investigated by Greisen and Nereson, the efficiency started to decrease appreciably at a distance of about 0.6 cm from the ends of the wire.

Again with the same method, Cosyns (CMG36) and Danforth and Ramsey (DWE36) measured the efficiency of Geiger-Mueller counters filled with different gases at different pressures. They compared the experimental data with the theoretical dependence of the efficiency on the gas density and were thus able to determine the primary specific ionization of cosmic-ray particles in various gases. Figure 2 shows the experimental

results obtained by Danforth and Ramsey along with the corresponding theoretical curves. Table 1 lists the values of  $j_p\rho_0$  obtained by this method;

Table 3.8.1. Experimental determination of the primary specific ionization of cosmic-ray particles by counter efficiency

AUTHORS	Gas	$j_p\rho_0$ ( $\text{cm}^{-1}$ )
Danforth and Ramsey	Air	21
Danforth and Ramsey	H <sub>2</sub>	6.2
Cosyns	H <sub>2</sub>	5.96
Cosyns	He	5.96
Cosyns	A	29.4

$\rho_0$  represents here the density of the gas at normal pressure and temperature. In interpreting the data in Table 1 and Fig. 2 one should note that the majority of cosmic-ray particles at sea level are  $\mu$ -mesons with

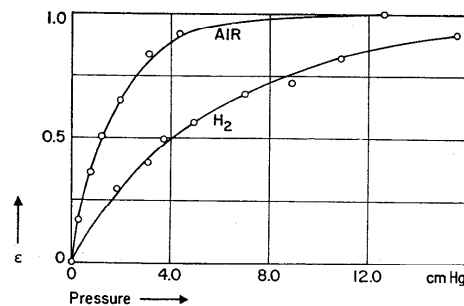


Fig. 3.8.2. Efficiency,  $\epsilon$ , of Geiger-Mueller tubes as a function of pressure for air and hydrogen, from Danforth and Ramsey (DWE36). The circles are experimental points. The curves represent theoretical efficiencies corresponding to values of  $j_p\rho_0$  of 21 ion pairs per centimeter in air and 0.2 ion pairs per centimeter in hydrogen (at normal temperature and pressure). In the computation of these curves the path length distribution of cosmic-ray particles in the tube was taken into consideration.

energies of the order of 10 times their rest energy. Therefore the experimental values for  $j_p\rho_0$  in hydrogen (6.2 and 5.96  $\text{cm}^{-1}$ ) may be compared with the theoretical value given by Eq. (2.10.1) with  $1/\sqrt{1-\beta^2} \approx 10$ . From this equation one obtains  $j_p\rho_0 = 5.2 \text{ cm}^{-1}$ .

Hereford (HFL48) measured the primary specific ionization in hydrogen of electrons with energies between 0.2 and 9.0 Mev using the  $\beta$ -ray spectrum

of radium and of  $B^{10}$ . In this experiment the electrons were collimated so that they all had the same path length in the Geiger-Mueller counter and Eq. (4) could be applied directly. In Fig. 3 the experimental results of Hereford are compared with the theoretical curve computed from Eq. (2.10.1). The agreement is satisfactory. In particular, the experimental results seem to confirm the existence of a minimum for the specific ionization, as predicted by the theory.

A particle of minimum ionization has a probability of the order of 0.5 per cent to traverse a Geiger-Mueller counter of the types ordinarily used without producing an ion pair. Often the inefficiency due to the dead time is also of the order of 0.5 per cent. Thus the overall inefficiency

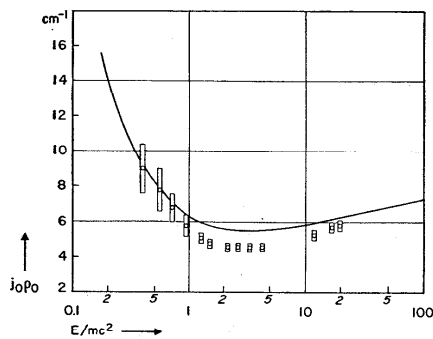


Fig. 3.8.3. Results of determinations of the primary specific ionization of electrons in hydrogen. The abscissa is the ratio  $E/mc^2$  of the kinetic energy to the rest energy. The ordinate is the number of ion pairs per centimeter at normal temperature and pressure. The curve is computed from Eq. (2.10.1). From Hereford (HFL48).

is usually of the order of 1 per cent; its exact value, of course, depends on the dimensions of the counter, on the gas filling, on the counting rate, on the sensitivity of the recording circuit, etc.

Air- or argon-filled counters with pressures of the order of one centimeter of mercury and hydrogen or helium-filled counters with pressures of the order of several centimeters of mercury have efficiencies that depend markedly on the specific ionization. Therefore, one can use such counters to separate particles with different specific ionization (HFL48). One obtains a sharper discrimination by using, instead of one, several low-pressure counters in coincidence. If  $\epsilon$  is the efficiency of a single counter, the efficiency of an  $n$ -fold coincidence array is  $\epsilon^n$ . The larger  $n$  becomes, the more  $\epsilon^n$  approaches a step function in its dependence on the specific ionization.

**3.9. The cloud chamber.\*** The operation of the cloud chamber is based upon the property of ions to act as nuclei for the formation of droplets from a supersaturated vapor. The cloud chamber consists essentially of a vessel containing a noncondensable gas saturated or almost saturated with a vapor, and built in such a way that its volume can be increased suddenly. The expansion causes the temperature of the mixture to drop, and consequently the vapor becomes supersaturated.

If the gas contains dust, a small expansion is sufficient to produce a general fog. This is due to the condensation of the vapor around the dust particles. If the gas is dust-free, no condensation occurs until the *expansion ratio* (i.e., the ratio of the volumes after and before expansion) reaches a minimum value, called the *ion limit*. Above this limit droplets begin to condense around whatever ions are present in the chamber. The droplets thus formed, under strong illumination, appear as brilliant points on a dark background. If one continues to increase the expansion ratio, one eventually reaches a condition known as the *cloud limit*, at which a dense cloud of very minute droplets appears throughout the chamber. A cloud chamber operated between the ion limit and the cloud limit reveals the trajectory of an ionizing particle by the array of droplets formed around the ions that are left by the ionizing particle in the gas of the chamber. This array, or *track*, can be observed visually. For quantitative work, however, it is recorded photographically.

A detailed theory of the formation and growth of droplets from a supersaturated vapor is still wanting. One can, however, understand the main features of the observed phenomena from the following considerations, developed originally by Lord Kelvin; see (DGN46).

Because of the surface tension, the vapor pressure is greater at the surface of a liquid drop than at a plane surface of the same liquid, and increases as the radius of the droplet decreases. A drop can grow only in a supersaturated vapor, and the degree of supersaturation necessary for the growth is greater the smaller the radius of the drop. It is likely that, in a vapor, minute droplets are formed continuously by the coalescence of vapor molecules. Because of their very small dimensions and the consequently large vapor pressure at their surface, these droplets evaporate immediately instead of condensing vapor from the surrounding gas, unless the vapor is very strongly supersaturated. Presumably the cloud limit corresponds to the degree of supersaturation necessary for condensation to occur around the droplets spontaneously formed by the coalescence of vapor molecules.

Below the cloud limit, the formation of droplets from a supersaturated vapor requires the presence of extraneous nuclei of condensation. As mentioned above, dust particles and ions provide such nuclei of condensa-

\* In ref. (DGN46) the reader will find a detailed discussion of the operation of cloud chambers and of their applications.

tion. Dust particles allow droplets to form with initial dimensions sufficiently large to require only a moderate degree of supersaturation for their growth. Ions favor condensation because their charge partially counteracts the effect of surface tension, allowing permanent drops of definite size to form about them in supersaturated vapor. These sub-visible drops then act as condensation nuclei when the vapor is moderately supersaturated.

The expansion ratio necessary to produce condensation on the ions depends on various factors. Since the gas expands very rapidly, one can neglect heat transfer during expansion. The temperatures,  $T_1$ ,  $T_2$ , before and after the expansion are then related to the corresponding volumes,  $V_1$ ,  $V_2$ , by the equation:

$$\frac{T_2}{T_1} = \left(\frac{V_1}{V_2}\right)^{\gamma-1} \quad (1)$$

where  $\gamma$  is the ratio of the specific heats at constant pressure and at constant volume for the gas mixture.

Equation (1) shows that the smaller  $\gamma$  is, the greater is the expansion ratio necessary to produce a certain temperature drop and, therefore, a certain degree of supersaturation. The value of  $\gamma$  is 1.40 for air and 1.66 for monoatomic gases, such as argon. Thus the necessary expansion ratio is smaller for a cloud chamber operating with argon than for one operating with air. The nature of the vapor also influences the operation of the cloud chamber markedly, and so does the value of the total pressure before expansion (in general, the degree of supersaturation for a given expansion ratio increases with increasing pressure).

Note that positive and negative ions are not equally effective as nuclei of condensation and that their relative effectiveness depends on the nature of the vapor. It was found, for example, that water condenses more readily on *negative* ions, methyl and ethyl alcohol condense more readily on *positive* ions, and benzene condenses as easily on positive as on negative ions.

**3.10. Design and operation of cloud chambers.** Experimenters have used cloud chambers in the shape of cylinders and of parallelepipeds, with linear dimensions ranging from about 10 centimeters to about 1 meter. The design of a cloud chamber depends on various considerations, among which the necessity of minimizing distortion of the tracks is very important.

One of the causes of distortions is the irregular motion of the various gas layers with respect to one another during the expansion. The difficulty of avoiding such irregular motions increases with increasing expansion ratio. It is therefore advisable to use gas mixtures for which the necessary expansion ratio is a minimum. Convection currents produced by differences of temperatures between various parts of the chamber also represent a common source of distortion

Different devices have been employed to expand the gas in a cloud chamber. The first cloud chamber designed by C. T. R. Wilson (WCT12) consisted of a glass cylinder closed at one end by a thick glass plate and at the other end by a piston. The motion of the piston produced the required expansion.

In a later model, again originated by C. T. R. Wilson (WCT33), the piston was replaced with a rubber diaphragm separating the chamber proper from an auxiliary back chamber. In a chamber of this type one produces the expansion by suddenly allowing part of the gas from the back chamber to escape into the atmosphere or into another vessel at an appropriate pressure. The decrease of the pressure in the rear chamber causes the diaphragm to move back, thus decreasing the pressure in the chamber proper. In order to minimize irregularities in the gas flow and to provide a suitable background, a perforated plate covered with black velvet is placed in front of the rubber diaphragm. In this type of chamber, the moving parts have a much smaller mechanical inertia than in the piston-type chamber, a feature of great importance for counter control (see below).

C. T. R. Wilson (WCT35) also developed a cylindrical cloud chamber with radial expansion. In this cloud chamber, the cylindrical wall is surrounded by an annular chamber and communicates with it through a large number of small openings. One produces the expansion by suddenly reducing the pressure in the annular chamber.

Cloud chambers have been operated with pressures from a fraction of an atmosphere up to 200 atmospheres.

In order to remove old ions, it is necessary to maintain an electric field (*clearing field*) in the chamber. This field may or may not be removed at the moment of the expansion.

The time sequence of the events in the operation of a cloud chamber is as follows. The expansion is usually completed in a time of the order of 10 milliseconds. If ions are present at the time of the expansion, condensation begins immediately. The droplets grow gradually in size until the supply of vapor in the immediate neighborhood of the ions is exhausted. The heat released by the condensation causes the temperature of the gas to rise slightly. The temperature of the gas then continues to rise through heat conduction from the walls of the chamber. Eventually the droplets, which, in the meantime, have fallen some distance below the place where they have been produced, re-evaporate. The chamber is not ready for another successful expansion until the evaporation of the droplets is completed and until both the temperature and the vapor pressure have again become uniform throughout the volume of the gas. The time necessary for this to happen is usually referred to as the *recycling time*. To accelerate the disappearance of old droplets and thereby shorten the recycling time, one may expand the chamber partially one or several times after each main expansion.

If no ions are present when the expansion occurs, the vapor remains in a supersaturated condition for a certain time, determined by the rate of heat flow from the walls of the chamber into the gas and by the heat capacity of the latter. If ions are formed in the gas during this time (the *sensitive time*), condensation will occur.

In a chamber operated at approximately atmospheric pressure the sensitive time is of the order of several hundredths to several tenths of a second, and the recycling time may vary from a fraction of a minute to several minutes. Both the sensitive time and the recycling time increase with increasing pressure. The picture of the track is taken by means of an intense light flash of microseconds duration 50 to 200 milliseconds after the beginning of the expansion. This time interval is chosen sufficiently long to allow the droplets to grow to a convenient size, yet sufficiently short to minimize distortion of the track due to the fall of the drops and to convection currents.

In order to be able to locate the tracks in space, one usually takes stereoscopic pictures of the cloud chamber. One can do this either by using two separate cameras with their objectives appropriately spaced, or by photographing the cloud chamber and its image upon a mirror with a single photographic camera.

In cosmic-ray experiments, cloud chambers sometimes are operated at random, but more often are *counter-controlled*; i.e., they are triggered by arrangements of Geiger-Mueller tubes that favor the recording of certain types of events. Counter-controlled chambers were first used by Blackett

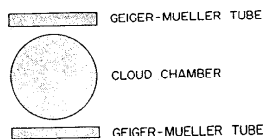


Fig. 3.10.1. Schematic arrangement of a counter-controlled cloud chamber.

and Occhialini (BPM33). Figure 1 shows schematically a typical example of such an arrangement. The chamber is expanded whenever a coincidence occurs between the pulses of two Geiger-Mueller tubes, placed one above and the other below the chamber. These coincidences are caused mainly by cosmic ray particles traversing the two counters and the chamber placed between them; therefore most of the cloud-chamber pictures taken with

this triggering arrangement show the tracks of single cosmic-ray particles (a cloud chamber suitable for counter control will be described in § 3.13).

In cloud-chamber experiments with artificially accelerated particles one often operates the accelerator so as to produce short pulses of radiation separated by long time intervals. One can then time-correlate the operation of the cloud chamber to that of the accelerator in such a way as to have the particles under investigation traverse the chamber either shortly before or shortly after the expansion, whichever is more appropriate for the specific purpose of the experiment.

**3.11. Post-expansion tracks. Measurement of the primary specific ionization.** When an ionizing particle traverses a cloud chamber shortly after an expansion has taken place, condensation occurs before the ions diffuse an appreciable distance. Under these circumstances, the drops that condense around the positive and negative ions coalesce, or, at least so do their images on the photographic film. A secondary electron of low energy that, on account of its small range, gives rise to a cluster of closely spaced ions, will appear on the film as a blob. Electrons of higher energy produce tracks branching off from the track of the primary particle, and the ionization of these secondary electrons can easily be distinguished from that produced directly by the primary particle. Thus, by counting the droplets along the track of the particle and disregarding the droplets along the secondary branches (which are rare) one obtains the number of primary ionizing events.

The method described above was used by Williams and Terroux (WEJ30) to determine the primary ionization of  $\beta$ -rays from radioactive sources. The energy of these rays was close to that corresponding to the minimum of the ionization curve. Information on the primary ionization of cosmic-ray particles was obtained by Kunze (KB33), Corson and Brode (CDR38), and Hazen (HWE43.1). The measurements of Hazen are probably the most accurate because of the number of tracks analyzed, because of the simultaneous measurements of specific ionization and momentum (see § 4.13 below), and because of the improved experimental technique.

Table 3.11.1. Experimental determination of the primary specific ionization by the cloud chamber method

AUTHOR	Gas	Particles	Momentum (ev/c)	$\rho_0 \sqrt{p}$ (cm <sup>-1</sup> )
Williams and Terroux (WEJ30)	H <sub>2</sub>	electrons	~10 <sup>8</sup>	6.4
	O <sub>2</sub>	electrons	~10 <sup>8</sup>	26
Kunze (KB33)	Air	mesons (?) (10 tracks)	~10 <sup>8</sup>	19
Corson and Brode (CDR38)	Air	mesons (?)	~10 <sup>8</sup>	14-18
Hazen (HWE43.1)	He	electrons* (21 tracks)	from 0.75 · 10 <sup>8</sup> to 9 · 10 <sup>8</sup>	6.6
Hazen (HWE43.1)	He	mesons* (25 tracks)	> 3 · 10 <sup>8</sup>	6.5

\* For momenta below 10<sup>8</sup> ev/c electrons can be safely distinguished from mesons because the specific ionization of the two kinds of particles differ by a large factor. Particles with momenta larger than 3 · 10<sup>8</sup> were considered to be  $\mu$ -mesons because it is known that, in this momentum range, most cosmic-ray particles are  $\mu$ -mesons.

The results of the various investigators are presented in Table 3.11.1. These results are in fair agreement with those obtained from the efficiency of Geiger-Mueller tubes (see Table 3.8.1). Note that the measurements of Hazen in helium give approximately the same value of  $j_p$  for electrons between  $0.75 \cdot 10^6$  and  $9 \cdot 10^6$  ev/c and for mesons above  $3 \cdot 10^8$  ev/c. Electrons of energy between  $0.75 \cdot 10^6$  and  $9 \cdot 10^6$  ev/c are close to the minimum of the ionization curve. The group of mesons investigated, however, includes a large proportion of high-energy particles, for which the theory predicts a specific ionization appreciably higher than minimum (about 8 ion pairs per cm if the value at the minimum is taken as 6.5). Experimental errors may possibly have hidden the expected difference.

The scarcity of data is due to the fact that since a cosmic ray must traverse the chamber *after* the expansion, counter control cannot be used. The probability that a cosmic ray traverses the chamber at just the right time to permit an accurate measurement of the primary ionization is very small.

**3.12. Pre-expansion tracks. Measurement of the probable specific ionization.** If an ionizing particle traverses a cloud chamber before the expansion, the ions will have diffused away from their point of production by the time condensation begins and the track will appear correspondingly broad. The density of droplets,  $\delta$ , at a distance  $y$  from the center of the track is given by the equation (BPM34)

$$\delta = \delta_0 e^{-y^2/4Dt}, \quad (1)$$

where  $\delta_0$  is the density at the center of the track,  $t$  is the time interval between the passage of the particle and the onset of the condensation, and  $D$  is the diffusion coefficient of the ions. Consider, for instance, the case that the chamber is filled with air. In air, electrons undergo attachment and the mean value of the diffusion coefficient for positive and negative ions,  $D$ , is  $0.034 \text{ cm}^2 \text{ sec}^{-2}$  at normal temperature and pressure. We may define as "width" of the track the width  $\Delta$  of a strip containing 90 per cent of all droplets. From Eq. (1) one obtains:

$$\Delta = 4.68\sqrt{Dt}. \quad (2)$$

When the cloud chamber is operated with counter control, there always is an unavoidable delay, of the order of  $10^{-2}$  seconds, between the passage of the particle and the expansion. The corresponding width of the track in a cloud chamber filled with air at normal temperature and pressure is about 0.09 cm. Ordinarily, an electronic device removes the clearing field within a few microseconds after the passage of the particle. In this case the positive and negative ions form a single track. If, however, the field is not removed, the positive and negative ions drift in opposite directions, giving rise to two separate tracks.

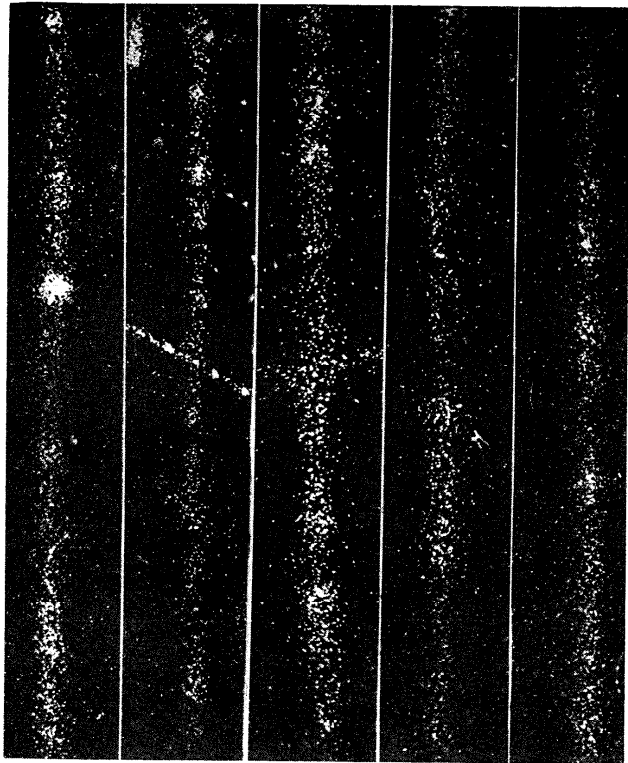


Fig. 3.12.1. Typical tracks of cosmic-ray particles obtained with a delay of 0.2 sec between the passage of the particle and the expansion of the chamber (reproduced double natural size). Note the separate droplets corresponding to individual ions and the clusters corresponding to the production of secondary electrons of several Kev energy. From Brode (BRB39).

The cloud-chamber technique provides the most direct method for measuring the probable specific ionization of charged particles (see § 2.10). For this purpose the chamber is expanded with a delay of 0.02 to 0.2 seconds after the passage of the particle. Under these conditions, the ions diffuse sufficiently far from one another so that a separate droplet forms



around each ion. A secondary electron of energy not sufficiently large to produce a separate track gives rise to a cluster of drops that can be resolved if it is not too dense; i.e., if the energy of the secondary electron is not too large (see Fig. 1). By counting all the droplets that occur singly or in clusters of not more than a certain number of drops, one can determine the number of ion pairs produced either directly or by secondary electrons of energy not larger than a certain value. This number is what we have defined as the probable specific ionization.

Clearly, in order to obtain reliable values for the probable specific ionization, one must control the operation of the cloud chamber very carefully. Indeed, as noted in § 3.9, by gradually increasing the expansion ratio one obtains first condensation on ions of one sign, then condensation on ions of the other sign, and eventually formation of spurious droplets. Lack of careful control explains the wide discrepancies in the early results of measurements by the method of droplet counting. The proper adjustment of the chamber is greatly facilitated if one does not remove the clearing field before the expansion, so that the positive and negative ions form separate tracks. If, for example, one uses alcohol as a vapor and adjusts the expansion so that about half of the droplets in the negative track are formed, one can be reasonably certain that the positive track is completely formed and that spurious droplets are not present in appreciable numbers.

Various investigators, including Brode (BRB39), Sen Gupta (SGR40), Hazen (HWE45), Skolil (SLL46), and Frost (FRH47) reported measurements of the specific ionization by the method of droplet counting. Most of these determinations refer to cosmic-ray particles and were made by means of counter-controlled cloud chambers. Depending on the experimental conditions (mainly on the delay between the passage of the ionizing particle and the expansion) the maximum size of cluster that could be resolved varied from about 20 to about 250 droplets. In the case that the positive and negative tracks are separated, the number of droplets in a cluster,  $N$ , is related to the energy of the secondary electron responsible for the cluster,  $\eta$ , by the relation:

$$\eta = NV_0, \quad (3)$$

where  $V_0$  is the energy per ion pair in the gas that fills the cloud chamber (see § 2.10).

The results of Hazen relative to electrons and mesons of various momenta in air are presented in Table 1. In these measurements, only clusters containing less than 19 droplets were counted. The corresponding limiting energy is  $\eta \approx 600$  ev. The particles in group (2) were identified as electrons either because they occurred in showers or because their specific ionization was less than one-half that predicted for mesons of the same momentum. The particles in groups (3) and (4) were identified as

Table 3.12.1. Values of the probable specific ionization of electrons and mesons in air, according to Hazen;  $\eta$  equals 600 ev

GROUP	Particles	$p$ (Mev/c)	$\rho_0 j_\eta$ (cm <sup>-1</sup> )	
			exper.	theor.
1	electrons ( $\beta$ -rays from $P^{32}$ )	1.35-2.1	$39 \pm 2$	39
2	electrons (cosmic rays)	30-240	$52 \pm 3$	53
3	mesons	210-600	$41 \pm 3$	39
4	mesons	> 210	$45 \pm 2$	46

mesons because they occurred singly under a lead shield, an event that is extremely improbable for high-energy electrons. Moreover, it is known from other experiments that at sea level electrons form only a small proportion of cosmic-ray particles above 200 Mev. The quantities listed in Table 1 are the products of the specific ionization,  $j_\eta$ , and the density of air,  $\rho_0$ . Thus they represent the numbers of ion pairs per centimeter. All values are reduced to dry air at normal temperature and pressure (this includes the correction for the additional ionization of the vapor present in the cloud chamber). The data are also corrected for the lack of resolution caused by overlap of the images of the droplets (this correction is of the order of 7 per cent).

Table 1 also contains the theoretical values of the product  $\rho_0 j_\eta$  for the various groups. The value for group (4) is an average figure based on the known momentum spectrum of cosmic-ray mesons. One sees that the experimental results agree satisfactorily with the theory. In particular, the measurements with electrons confirm the slow increase of specific ionization with energy that is theoretically predicted from the relativistic deformation of the electric field of a rapidly moving particle.

A quantity of interest is the value of the specific ionization at the minimum. Table 2 summarizes the results of Hazen (for mesons in air) and those of Frost (FRH47), as reported by Brode (BRD49) for mesons and electrons in various gases. In these experiments the largest clusters considered had 25 droplets. The theoretical determinations of  $\rho_0 j_\eta$  are based upon Eqs. (2.5.1) and (2.10.2) and upon the values of the energy per ion pair,  $V_0$ , listed in the third column. The quantity  $V_0$  is not known accurately. Moreover, the validity of Eq. (2.5.1), giving the collision loss by distant collisions, is here somewhat questionable, because the binding energies of the electrons in the innermost atomic shells of air and argon are greater than the chosen limiting energies,  $\eta$ . For these reasons, the theoretical values of the specific ionization are somewhat uncertain. This uncertainty, however, does not affect the relative values of the probable

specific ionization of different particles in any given gas. The fact that the experimental minimum values of the probable specific ionization of mesons and electrons in each gas are closely the same is thus significant and it may be regarded as direct evidence for the equality of the charges of these particles.

Table 3.12.2. Values of the minimum probable specific ionization of mesons and electrons in various gases (in ion pairs per centimeter at normal pressure and temperature).

AUTHOR	Gas	$V_0$ (ev)	$\eta$ (ev)	Particles	$\rho_{j_0}$ ( $\text{cm}^{-1}$ )	
					exper.	theor.
Hazen (HWE45)	Air	33	870	mesons	38	44
Frost (FRH47)	H <sub>2</sub>	31	770	electrons	$6.48 \pm 0.34$	7.8
Frost (FRH47)	H <sub>2</sub>	31	770	mesons	$6.78 \pm 0.34$	7.8
Frost (FRH47)	He	26	650	electrons	$8.13 \pm 0.51$	8.1
Frost (FRH47)	He	26	650	mesons	$8.20 \pm 0.41$	8.1
Frost (FRH47)	A	24	570	electrons	$53.1 \pm 2.8$	62.0
Frost (FRH47)	A	24	570	mesons	$55.0 \pm 2.8$	62.0

**3.13. Momentum measurements.** The cloud-chamber technique affords the possibility of measuring directly the momenta of charged particles. For this purpose, one operates the cloud chamber in a uniform magnetic field and measures the curvature of the tracks.

The magnetic field may be produced by a pair of Helmholtz coils, by a permanent magnet, or by an electromagnet. If one uses a magnet, the view of the cloud chamber is obstructed by one of the pole pieces, and special devices are necessary in order to photograph the tracks. For example, one can place a mirror at  $45^\circ$  in front of the cloud chamber, within the gap of the magnet. Or one can drill a conical hole in one of the pole pieces, with the wider aperture facing the chamber.

Figure 1 shows, as an example, the magnet chamber used by Blackett (BPM34). Its description follows, in the words of the author:

"The whole object of the design was to reduce, as far as possible, the gap between the pole pieces. For, provided the iron is not nearly saturated, the field obtained is inversely proportional to this gap

"As no piston rod could conveniently be used, the piston A was unsupported except by the rubber diaphragm which served to close the chamber. When in the upper position, the piston rested against three brass stops, B. When in the expanded position it lay flat on a rubber covered iron plate, C. The expansion was changed by altering the position of this iron plate. This was done by means of three long screws, D, with coned ends, E, on which the iron plate rested. The main casting was of brass, but an iron plate G was let into the back so as to form a continuation of the pole piece. Since the top of the iron plate, C, was effectively the pole face, this device enabled the tracks to be photographed within less than a centimeter of the pole face.

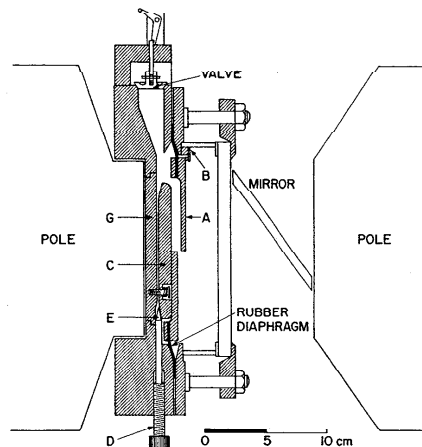


Fig. 3.13.1. A cloud chamber designed by Blackett for use in the field of an electromagnet (BPM34).

"The tracks were photographed by two cameras, using a mirror at an angle of about  $45^\circ$ ."

The equation of motion of a particle of charge  $ze$ , velocity  $\mathbf{v}$ , and momentum  $\mathbf{p}$  in a magnetic field  $\mathcal{B}$  is:

$$\frac{d\mathbf{p}}{dt} = \frac{ze}{c} \mathbf{v} \times \mathcal{B}, \quad (1)$$

where the mechanical quantities are measured in the CGS system,  $\mathcal{B}$  is measured in gauss, and  $e$  is the charge of the electron in electrostatic units. From Eq. (1), which is relativistically correct, it immediately follows that the absolute value of the momentum of the particle remains constant (since  $d\mathbf{p}/dt$  is perpendicular to  $\mathbf{v}$ , and therefore to  $\mathbf{p}$ ) and that, if  $\mathcal{B}$  is constant, the particle describes a helicoidal path on a cylinder whose axis is parallel to the magnetic field (since the component of  $\mathbf{p}$  parallel to the field does not change). The radius,  $R$ , of this cylinder is given by the equation:

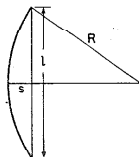
$$\frac{pc}{ze} \sin \theta = R\mathcal{B}, \quad (2)$$

where  $\theta$  is the angle between the magnetic field and the trajectory. If, in particular,  $\theta = \pi/2$  (as is often nearly the case):

$$\frac{pc}{ze} = R\mathcal{B}. \quad (3)$$

The quantity  $R\mathfrak{B}$  is often referred to as "magnetic rigidity." According to Eq. (3) it is proportional to  $p/z$ ; it has the dimensions of an electric potential and is measured in electrostatic units. The quantity  $300zR\mathfrak{B} = 300pc/e$  represents an electric potential measured in volts. It is proportional to  $p$  and is known as the momentum of the particle in  $ev/c$  (see Appendix 1).

Fig. 3.13.2. Determination of the curvature of a cloud-chamber track.



Usually the accuracy in the determination of the momentum is limited by the experimental uncertainty in the value of  $R$ . For the evaluation of the error in the measurement of  $R$  it is necessary to specify the method employed for this measurement. We shall assume here that one determines the radius  $R$  by selecting a section of the trajectory of length  $l$  and measuring the corresponding sagitta,  $s$  (see Fig. 2). If  $s \ll R$ ,  $R$  is given by the equation:

$$R = \frac{l^2}{8s} \quad (4)$$

and  $p$  by the equation:

$$\frac{pc}{e} = \frac{l^2\mathfrak{B}}{8s} \quad (5)$$

The experimental error in the measurement of  $s$  depends (a) on instrumental factors like finite width of the track, optical distortions, and distortions caused by convection currents; and (b) on the multiple Coulomb scattering of the trajectory in the gas of the chamber.

The instrumental error,  $(\delta p)_i$ , is independent of the momentum of the particle. One can determine its average value by measuring the apparent average curvature of the tracks of very-high-energy particles (for which scattering is negligible) in the absence of a magnetic field. The corresponding apparent momentum,  $p_0$ , in a field  $\mathfrak{B}$  is given by the equation

$$\frac{p_0c}{e} = \frac{l^2\mathfrak{B}}{8(\delta s)_i} \quad (6)$$

and is called the *maximum detectable momentum*. Considering that, in absolute value,  $\delta p/p = \delta s/s$ , one can express the relative uncertainty in the value of the momentum due to instrumental errors in terms of the maximum detectable momentum, as follows:

$$\left(\frac{\delta p}{p}\right)_i = \frac{p}{p_0} \quad (7)$$

The standard error in the measurement of the sagitta,  $s$ , due to scattering can be obtained from Eqs. (2.17.13) and (2.16.7). It has the value:

$$(\delta s)_s = \frac{1}{4\sqrt{6}} \frac{E_s l}{pc\mathfrak{B}} \sqrt{\frac{l\rho}{X_0}} \quad (8)$$

where  $\rho$  is the density of the gas and  $X_0$  the radiation length. The corresponding relative error in the measurement of the momentum may be expressed as follows:

$$\left(\frac{\delta p}{p}\right)_s = \frac{\mathfrak{B}_s}{\mathfrak{B}} \quad (9)$$

where

$$\mathfrak{B}_s = \sqrt{\frac{2}{3}} \frac{E_s}{c\mathfrak{B}} \sqrt{\frac{\rho}{lX_0}} \quad (10)$$

represents the velocity of the particle at which the apparent curvature caused by scattering equals that caused by the magnetic field.\*

One will notice that the instrumental error increases with increasing momentum, whereas the scattering error varies in the opposite sense for sub-relativistic velocities (and becomes independent of  $p$  when  $\mathfrak{B}$  is close to 1). For each type of particle and for each experimental arrangement, therefore, momentum measurements by the magnetic deflection method are only possible within a limited range of momenta. Consider, for instance, momentum measurements on  $\mu$ -mesons ( $m = 209m_e$ ) by means of a cloud chamber filled with argon at atmospheric pressure and operated in a magnetic field of 10,000 gauss. Assume that the average length of the cloud-chamber track is 20 cm and that instrumental errors set a limit of 0.05 cm to the accuracy in the measurement of the sagitta. From Eq. (6) one obtains a value of  $3 \cdot 10^9$   $ev/c$  for the maximum detectable momentum. Equation (10) gives  $\mathfrak{B}_s = 0.012$ ; the corresponding momentum is  $1.3 \cdot 10^6$   $ev/c$ . Thus the measurements are meaningful only for mesons with momenta small compared with  $3 \cdot 10^9$   $ev/c$  and large compared with  $1.3 \cdot 10^6$   $ev/c$ .

**3.14. Detection of ionizing particles by means of photographic emulsions.** Since 1910 it has been known that grains of silver halide in photographic emulsions became sometimes developable when traversed by ionizing particles (KS10; RM11). Thus, under certain conditions that will be discussed below, microscopic inspection of a plate that has been exposed to the passage of ionizing particles and subsequently developed reveals rows of silver grains outlining the trajectories of the ionizing particles.

\* For a more detailed description of the trajectories of particles under the combined effects of magnetic deflection and scattering see refs. (SWT49), (SWT50.1), and (GG50).

The probability,  $P$ , that the passage of an ionizing particle through a grain of silver halide makes the grain developable depends on the energy dissipated in the grain and is therefore a function of the specific energy loss,  $k$ , of the particle. For small values of  $k$ ,  $P$  is closely proportional to  $k$ . However, as  $k$  increases, the rate of increase of  $P$  becomes progressively slower, which seems to indicate that  $P$  approaches the limiting value of one asymptotically (see Fig. 1).

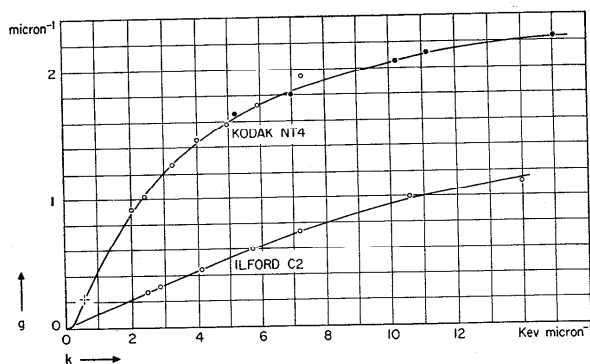


Fig. 3.14.1. Relation between the total collision loss,  $k$ , of a particle and the grain density,  $g$ , in the track. Points marked with open circles have been deduced from observations of  $\mu$  meson tracks; those marked with solid dots from similar measurements with protons. The point marked with a cross corresponds to particles of minimum ionization. From Brown *et al.* (BRH49.2).

The specific energy loss,  $k$ , considered here includes the energy going directly into excitation and ionization of atoms. It also includes a portion of the energy going into the production of secondary electrons; namely that portion which the secondary electrons dissipate within the grains of silver bromide where they are produced. It does not include radiation losses because a negligible fraction of the energy going into photons is re-absorbed in the grain where the radiation process occurs. Thus, for particles of low or moderately high energies, one may take  $k = k_{\text{col}(<\eta)}$  (see § 2.5), where  $\eta$  is the energy of an electron with range equal to the average linear dimensions of the grains. This energy is of the order of 5,000 or 10,000 ev.

At very high energies, a fraction of the energy loss by distant collisions,  $k_{\text{col}(<\eta)}$ , goes into Cerenkov radiation (§ 2.0) which partially escapes from the grains of silver bromide traversed by the ionizing particle. It is thus uncertain whether or not one should theoretically expect any relativistic in-

crease of  $P$  similar to the relativistic increase of  $k_{\text{col}(<\eta)}$  (MH50.2; SBM51). Experimentally, too, the existence of this effect appears doubtful (OGP49; PE50). It is certain, however, that, beyond the minimum,  $P$  increases only slightly, if at all, with increasing particle energy.

Blau (BM49) has presented some theoretical arguments suggesting for  $P(k)$  an expression of the following form:

$$P(k) = 1 - e^{-bk^{1/2}} \quad (1)$$

where  $k$  represents the energy loss of the particle per g  $\text{cm}^{-2}$  of the silver halide and  $b$  is a constant that depends on the dimensions of the grain and on the chemical composition of the emulsion. Experiments confirm the approximate validity of this expression, except, perhaps, in the case of the most sensitive emulsions.

The grain density along the track,  $g$ , i.e., the number of silver grains per unit length, is equal to  $P(k)$  times the cross-sectional area of the grains, times the number of grains per unit volume of the emulsion. In photographic emulsions one always finds, after development, a general background of silver grains distributed more or less at random. In order to distinguish a track against this background, it is necessary that the separation of the grains along the track be smaller than the average distance between the grains of the background. Therefore a given photographic emulsion will detect charged particles only with a specific energy loss,  $k$ , greater than a certain value  $k_1$ .

The sensitivity of a photographic emulsion for the detection of ionizing particles is often described by the ratio  $k_1/k_0$ , where  $k_0$  is the minimum value for the energy loss of a charged particle in the material under consideration. This corresponds to the energy loss of a singly charged particle with kinetic energy of the order of the rest energy (see § 2.5). Instead of speaking of the energy loss, one often speaks of the specific ionization, a quantity proportional to the energy loss (see § 2.10); and one thus describes a photographic emulsion as capable of detecting particles with " $n$  times minimum ionization." In the sub-relativistic region, the specific ionization and the energy loss are decreasing functions of the ratio  $E/mc^2$  of the kinetic energy to the rest energy. Therefore one can also characterize the sensitivity of a photographic emulsion by the maximum value of  $E/mc^2$  for a singly charged particle that leaves a detectable track.

Ordinary photographic plates are not well suited for the detection of ionizing particles. In ordinary plates the minimum detectable ionization is of the order of one hundred times the minimum ionization, so that only alpha particles and other multiply charged nuclei of low energy leave easily recognizable tracks. Moreover the emulsions are only a few microns thick, so that a particle must traverse the emulsion at a glancing angle in order to record a track of any appreciable length.

Myssowsky and Tschijow (ML27) in 1927 showed that one could use, for the detection of ionizing particles, emulsions considerably thicker

than the ordinary optical emulsions. As for the sensitivity, an obvious method of improvement consists of increasing the proportion of silver halide to gelatine, so as to increase the number of grains traversed by the ionizing particles per unit path length. Moreover, by proper chemical treatment of the emulsion, it is possible to "sensitize" the silver halide grains, i.e., to increase the probability that a grain becomes developable when traversed by a particle of given specific ionization (BM32). It is also possible to increase the sensitivity by an appropriate choice of the grain size (ZAP35).

Since the late 'thirties, a number of emulsions have been commercially prepared for the specific purpose of detecting ionizing particles. Photographic emulsions are now available with thicknesses up to 1200 microns. The proportion of silver halide in some of these emulsions is as large as about 80 per cent in weight.

A commercial emulsion that has been widely used is the Nuclear Research emulsion, developed by the Ilford Laboratories with the collaboration of C. F. Powell and G. P. S. Occhialini of the University of Bristol, England. The density of this emulsion is about  $4 \text{ g cm}^{-3}$ , of which about  $3.3 \text{ g cm}^{-3}$  are accounted for by "heavy" elements (Ag, Br, and I). Table 1 shows its composition. The Ilford Nuclear Research emulsion is prepared with different grain sizes, ranging from 0.4 microns (type B) to 0.1 microns (type D). The sensitivity varies greatly with grain size. Thus the "type B" emulsion is capable of recording protons up to about 100 Mev energy, whereas the "type D" emulsion can record only fission fragments.

Table 3.14.1. Composition of Ilford emulsions

ELEMENT	Z	$\text{g cm}^{-3}$	Atoms per $\text{cm}^3 \cdot 10^{-23}$	% in grams	% in atoms
I	53	0.053	0.0025	1.32	0.3
Ag	47	1.87	0.1049	46.67	12.4
Br	35	1.30	0.1090	33.05	12.18
S	16	0.014	0.0026	0.35	0.31
O	8	0.24	0.0909	5.91	10.75
N	7	0.030	0.0350	2.07	4.95
C	6	0.33	0.167	8.24	19.69
H	1	0.056	0.342	1.4	40.13
Ca, F, Cr, Si, Na		traces			

In 1948 the Kodak Laboratories produced the first emulsion capable of recording particles with minimum ionization. The sensitivity of this emulsion, called emulsion NT4, is compared with that of the Ilford C2 emulsion in Fig. 1 giving grain density as a function of energy loss for the two types of emulsions. One will notice that the curve corresponding

to the Kodak NT4 emulsion approaches saturation at values of  $k$  at which the other curve still rises in an almost linear fashion. Other emulsions of sensitivity comparable to that of the Kodak NT4 emulsion are now available. Among these, widely used is the Ilford G5 emulsion.

In what follows we shall call "electron-sensitive emulsion" an emulsion capable of detecting particles with minimum ionization and "electron-insensitive emulsion" an emulsion that does not have such property. These expressions are justified by the fact that emulsions insensitive to particles with nearly minimum ionization can never detect high-energy electrons and only under particularly favorable circumstances are able to detect low-energy electrons. For example, an electron of more than 50 keV energy does not produce a track of detectable grain density in an Ilford C2 emulsion. An electron of less than 50 keV energy, on the other hand, has a range of less than 10 microns and produces fewer than 5 silver grains. Moreover, these grains are not arranged on a straight line, because of the large scattering of low-energy electrons, and are therefore difficult to recognize against the general background.

A detailed description of the delicate methods employed for processing photographic emulsions after exposure goes beyond the scope of this volume. One should mention, however, that the difficulty of obtaining uniform development throughout the emulsion increases rapidly with increasing thickness. Indeed, the processing of emulsions thicker than about 100 microns requires special techniques, such as those described by Dilworth, Occhialini, and Payne (DCC48). This method takes advantage of the fact that the reduction of the silver bromide proceeds extremely slowly in a cold developing solution. Therefore one can obtain uniform development of a thick emulsion by first allowing the plate to soak in a cold developer until it becomes uniformly imbued with it and then raising the temperature to the point at which reduction occurs.\*

An important technical detail to be noted is the possibility of using "stripped emulsions," namely emulsions without glass backing. In a stripped emulsion the developer penetrates from both sides simultaneously. As a result, it turns out that a stripped emulsion of a given thickness can be developed as easily as a glass-backed emulsion of about one-quarter this thickness. Also, one can expose a number of stripped emulsions one next to the other, so as to form a layer of any desired thickness, and then develop them separately.

A source of error that may be serious in quantitative work with photographic emulsions is the gradual *fading* of the latent image. It has been found that the grain density along the track of an ionizing particle in a photographic emulsion decreases gradually as the time between exposure and development increases. The rate of fading varies greatly with the

\* Another method that gives good results for thickness up to about 200 microns has been described by Blau and DeFelice (BM48).

type of emulsion. It is also strongly affected by physical factors, such as the temperature and the humidity of the air in which the plates are kept. In Ilford C2 emulsion, used under ordinary conditions of temperature and humidity, appreciable fading occurs in a period of the order of one month. This means that in plates developed after about one month from exposure the tracks of the more heavily ionizing particles appear considerably thinner than in plates developed immediately after the exposure, and the tracks of less heavily ionizing particles may have disappeared altogether.

Another technical problem is the microscopic observation of the tracks. This includes the problem of finding the tracks (scanning) and the problem of making accurate measurements on these tracks (see § 3.15 below). For scanning one generally uses fairly low magnification, so as to increase both the field and the focal depth. For the actual measurements one uses high magnification. In this case, only small sections of each track can be brought to focus at any one time. Therefore the record of an event occurring in the photographic emulsion is usually obtained in the form of a mosaic of a large number of separate microphotographs (see Fig. 3.15.1).

### 3.15. Measurements on tracks in photographic emulsions.

Figure 1 shows microphotographs of the tracks of a number of different particles in nuclear emulsions. The aspect of these tracks varies greatly one from another. In some tracks the grain density is so large as to give the appearance of a solid line. Other tracks, instead, look like tenuous arrays of widely separated silver grains. Some tracks appear completely straight, while others show various degrees of scattering. The considerable width and the peculiar "hairy" structure of the tracks of heavy nuclei is due to the abundant production of secondary low-energy electrons, or  $\delta$ -rays.

Under favorable circumstances, the grain density, the scattering, and the frequency of  $\delta$ -rays lend themselves to quantitative measurements. These measurements, together with the determination of the range (whenever such determination is possible) furnish important information on the properties of the particles responsible for the tracks.

(a) *Grain Density.* Whenever the grains appear separate, one can measure the grain density by simply counting the number of grains per

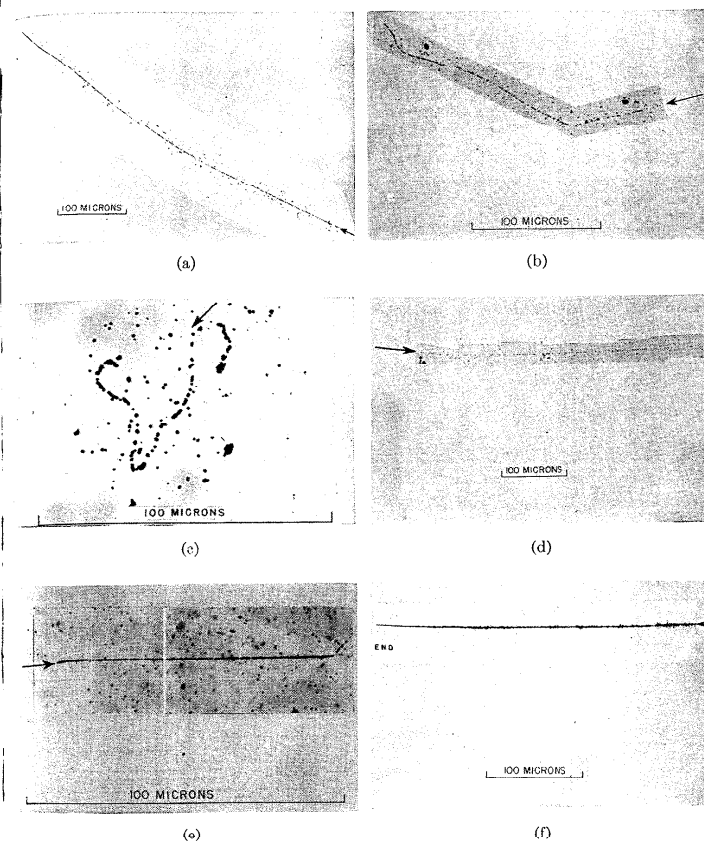


Fig. 3.15.1. (See caption bottom of page 132.)

Fig. 3.15.1. Tracks of various kinds of particles in photographic emulsions:

- (a) Proton stopping in Ilford C2 emulsion. Courtesy of B. T. Feld.
- (b) Meson stopping in Ilford C2 emulsion. Powell and Occhialini (*Nuclear Physics in Photographs*, Clarendon Press, Oxford 1947).
- (c) Low-energy electron stopping in Kodak NT4 emulsion. Brown *et al.* (BRH49.2).
- (d) Singly-charged relativistic particle (electron) traversing a Kodak NT4 emulsion. Brown *et al.* (BRH49.2).
- (e)  $\alpha$ -particle stopping in Ilford C2 emulsion. Courtesy of D. H. Perkins.
- (f) Nucleus (of atomic number  $Z = 19 \pm 2$ ) stopping in Ilford C2 emulsion. Bradt and Peters (BHL4S).

unit length of the track. As explained in the preceding section, the grain density is a function of the collision loss of the particle (see Fig. 3.14.1). For particles with unit charge, the collision loss, in turn, is a function of the velocity alone. Thus a measurement of the grain density gives, in principle, at least, the velocity of the particle (see § 2.5). Since one cannot compute the absolute value of the grain density corresponding to a given velocity, the plate must be calibrated with particles of known velocity. Because of the fading and because of the influence of processing upon the grain density, it is best to use, for calibration purposes, tracks appearing in the same plate and produced at the same time as the track under investigation.

For a nucleus with  $z$  units of charge, the theory predicts a collision loss  $z^2$  times greater than the collision loss of singly charged particles of the same velocity (see § 2.5). This law is well verified at high energies, but fails when the velocity of a multiply charged nucleus approaches the velocity of atomic electrons. The reason is that at these low velocities the nucleus attracts electrons into its orbit and travels part of the time as a partially ionized atom.

(b) *Range*. When the particle stops in the emulsion, one can measure the residual range,  $R$ , at any point of the trajectory by measuring, *along the trajectory*, the distance to the point where the particle comes to rest.

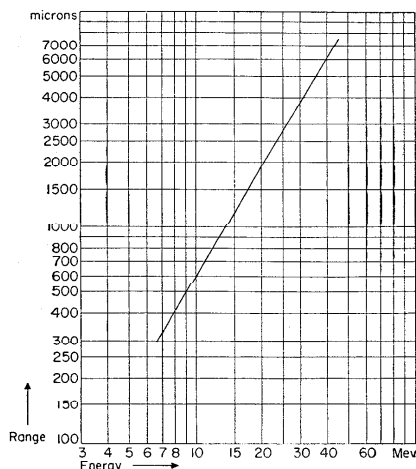


Fig. 3.15.2. Range-energy relation for protons in Ilford C2 emulsion. From Bradner *et al.* (BH50.1).

For particles with unit charge, the ratio  $R/m$  of range to mass is a function of the velocity alone, i.e., a function of the ratio  $E/m$  of energy to mass (see § 2.8). Thus one can compute the range-energy relation for particles with unit charge and arbitrary mass if one knows the range-energy relation for protons.

The energy-range relation for protons in the Ilford C2 emulsion is shown in Fig. 2. One sees that this relation may be approximated, over wide energy intervals by an expression of the form:

$$R = AE^\alpha, \quad (1)$$

where  $R$  is the range,  $E$  the kinetic energy and  $\alpha$  and  $A$  are constants. It follows from the arguments presented above that the range-energy relation for a particle of unit charge and arbitrary mass may be written as:

$$\frac{R}{m} M_p = A \left( \frac{E}{m} M_p \right)^\alpha, \quad (2)$$

where  $M_p$  is the proton mass and  $m$  the mass of the particle in question.

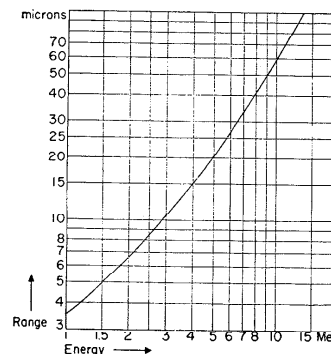


Fig. 3.15.3. Range-energy relation for  $\alpha$ -particles in Ilford C2 emulsion. From Lattes *et al.* (LCM47.3).

For a particle of mass  $m$  and charge  $ze$ , the ratio  $R/m$  is theoretically given by  $1/z^2$  times the value of  $R/m$  for a singly charged particle of the same velocity (see § 2.8). This theoretical result holds quite accurately for particles of high energies. In the low-energy region, however, the ranges of multiply charged nuclei are greater than the theoretical ones. As indicated above, this is due to the fact that, at low energies, capture of electrons lowers the effective charge of these nuclei. Figure 3 gives the energy-range relation for  $\alpha$ -particles in the Ilford C2 emulsion, as determined experimentally by Lattes and his collaborators (LCM47.3).

(c) *Scattering.* According to the theory of multiple scattering presented in § 2.16, the root mean square angle of scattering of a singly charged particle over a given distance is inversely proportional to the product  $\beta cp$  of the velocity times the momentum of the particle. For velocities small compared with the velocity of light,  $\beta cp \approx 2E$  where  $E$  is the kinetic energy. In this case, a measurement of the root mean square angle of scattering yields the kinetic energy of the particle. For velocities close to the velocity of light, a measurement of the mean angle of scattering yields the momentum.

In principle, the simplest method of determining the root mean square angle of scattering would be to draw the tangents to the trajectory at a number of equidistant points and to measure the angles between one tangent and the next. This, however, cannot be done because, in general, a track is not a smooth line but a discontinuous array of grains. To consider the line connecting the centers of two successive grains as the tangent would introduce large errors because the size of the silver grains is not small compared with their separation, and the particle may have traversed the grain at any point.

For the quantitative study of scattering, one may use two methods, which can be termed the "angular method" and the "sagitta method."

In the angular method (GCY48; GCY50) one obtains the average directions of successive segments of the track by allowing a straight line to pass as closely as possible to the centers of gravity of the grains in each segment. One measures, in absolute value, the angles, projected in the plane of the emulsion, between alternate segments and one then computes the arithmetic mean of these angles,  $|\theta_a|_{av}$ . One can do the measurement most conveniently by using a straight-line reticle in the eye-piece of a microscope fitted with a precise goniometer.

In the sagitta method (FPH50) one determines, at regular intervals, the distance of the track from a straight reference line. One can easily see that the mean second difference between these distances is proportional to the mean angle between successive chords to the track,  $|\theta_c|_{av}$ . To perform the measurement, one places the plate on the mechanical stage of the microscope, so that the track is approximately parallel to one of the lines of motion of the stage, say the  $X$ -axis. By means of an eye-piece scale, one then determines the ordinates,  $Y$ , of the points where the image of the track intersects a hair-line in the eye-piece.

One can prove that, under the Gaussian approximation, the mean angles,  $|\theta_a|_{av}$  and  $|\theta_c|_{av}$ , thus determined are respectively  $0.96\sqrt{\pi}$  and  $\sqrt{2\pi/3}$  times the root mean square angle of scattering in the length of one segment. Their expressions, therefore, are given by the following equations [see Eq. (2.16.10)]:

$$\frac{|\theta_a|_{av}}{0.96\sqrt{\pi}} = \frac{|\theta_c|_{av}}{\sqrt{2\pi/3}} = \sqrt{\frac{1}{2}} O_s \sqrt{d}, \quad (3)$$

where  $d$  is the length of one segment in  $\text{g cm}^{-2}$  and  $O_s$  is given by Eq. (2.16.3). Since  $O_s$  is inversely proportional to  $\beta p$ , one can write Eqs. (3) as follows:

$$\frac{|\theta_a|_{av}}{0.96\sqrt{\pi}} = \frac{|\theta_c|_{av}}{\sqrt{2\pi/3}} = \frac{D\sqrt{d}}{\beta p}, \quad (4)$$

where  $D$  is a constant that depends on the composition of the photographic emulsion.

One obtains best results by considering only scattering angles smaller than a given value. In this way one rules out those few large-angle deflections whose inclusion would introduce unnecessarily large statistical fluctuations. The maximum value of the angle considered in the analysis of the experimental results enters, of course, in the computation of the constant  $D$  in Eq. (4).

The two methods of measurement yield results of similar precision; the sagitta method, however, is somewhat faster at moderate energies. If the stage of the microscope is provided with a suitable movement, one can determine values of  $\beta cp$  up to several Bev with fair accuracy on long tracks.

The expressions for  $|\theta_a|_{av}$  and  $|\theta_c|_{av}$  given above are only approximate. One can obtain more accurate expressions on the basis of Moliere's theory (see § 2.17). One should also consider the fact that the various measurements from which one determines the value of the mean scattering angle are not statistically independent. The rigorous theory shows that the "scattering parameter,"  $D$ , is not exactly a constant, but varies slowly both with the momentum,  $p$ , of the particle and with the length,  $d$ , of the segments. We refer the reader to the papers of Goldschmidt-Clermont (GCY50) and of Moliere (MG51) for a detailed discussion of these questions. Here we wish to mention that experimental results of the Bristol group (GK51) confirm the dependence of  $D$  on  $p$  and  $d$  predicted by the theory and also check, in absolute value, the theoretical expression of this quantity. Thus one may regard the results of scattering measurements in photographic emulsions as a direct test of the theory of Coulomb scattering.

Before leaving this subject, we note that, under exceptionally favorable circumstances, it has been possible to measure momenta of the order of  $10^{11}$   $\text{ev}/c$  by a different application of the scattering method (see, e.g., § 8.20).

(d) *Delta Rays.* Delta rays are produced abundantly only by particles of sub-relativistic velocities. For these particles the maximum energy of the secondary electrons is approximately

$$E'_m = 2m_e c^2 \beta^2, \quad (5)$$

where  $\beta c$  is the velocity of the primary particle [see Eq. (2.2.7)]. The number per  $\text{g cm}^{-2}$  of  $\delta$ -rays with energies between  $E'$  and  $E' + dE'$  ( $E' < E'_m$ )



is given with sufficient approximation by the Rutherford formula, Eq. (2.4.14):

$$\Phi_{\text{sec}}(E, E') dE' = \frac{2Cm_e c^2 z^2}{\beta^2} \frac{dE'}{(E')^3}, \quad (6)$$

where  $z$  is the charge of the primary particle in terms of the charge of the electron.

Secondary electrons can be detected only when their energy lies within certain limits. The lower limit,  $E'_1$ , is determined by the requirement that the secondary electron should produce a track of at least 3 or 4 grains. The upper limit,  $E'_2$ , is often determined by the sensitivity of the emulsion. In the case of Ilford C2 plates, for example,  $E'_1$  is of the order of  $10^4$  ev and  $E'_2$  of the order of  $3 \cdot 10^4$  ev (BHL48).

Comparison of the experimental data with the theoretical formula (6) shows that, even in the energy range between  $E'_1$  and  $E'_2$ , most of the secondary electrons escape detection. However, the fraction of secondary electrons detected with a given emulsion appears to be fairly constant. (This fraction is of the order of 10 per cent for the Ilford C2 emulsion). Therefore the observed number of  $\delta$ -rays per unit length,  $n_\delta$ , is given by an equation of the following type, obtained by integration of Eq. (6):

$$n_\delta = H \frac{z^2}{\beta^2} \left( \frac{m_e c^2}{E'_1} - \frac{m_e c^2}{E'_{\text{max}}} \right), \quad (7)$$

where  $E'_{\text{max}}$  equals  $E'_m$  or  $E'_2$ , whichever is smaller, and  $H$  is an empirical constant to be determined by  $\delta$ -ray counting on a track of a particle with known charge and velocity. When  $E'_m > E'_2$ ,  $n_\delta$  varies as  $z^2/\beta^2$ ; thus a measurement of the frequency of  $\delta$ -rays gives the same information as a measurement of the grain density. The two methods are, to a certain extent, complementary. One can use grain counting for small values of the ratio  $z^2/\beta^2$ ,  $\delta$ -ray counting for large values of the same ratio. In both cases the measurements yield the value of  $z^2/\beta^2$  for the particle under consideration relative to the value of the same quantity for a particle of known  $z$  and  $\beta$ .

(e) *Magnetic Deflection.* Recently Dilworth and her collaborators (DCC50.2) have exposed plates in a 35,000-gauss magnetic field and obtained sufficient magnetic deflection to establish the sign of the particle when the track is more than 5,000 microns long. It is hardly necessary to note that, because of the very large scattering error, magnetic deflection in photographic emulsions does not yield an accurate determination of the momentum.

### 3.16. Identification of tracks in photographic emulsions.

When an ionizing particle comes to rest in the emulsion of a photographic plate, a measurement of its range together with a determination of either the grain density, the scattering, or the frequency of  $\delta$ -rays along the track often affords unambiguous identification of the particle. Indeed, observa-

tions of this kind led to the discovery of a previously unknown particle (the  $\pi$ -meson; see § 4.8). Under favorable circumstances one can also estimate the mass of a particle that does not stop in the emulsion, from measurements of grain density and scattering.

(a) *Mass Determinations of Singly Charged Particles from Range and Grain Count (LCM48).* For a given residual range, the grain density along the track of a singly charged particle is an increasing function of its mass. In principle the simplest method for comparing the masses of two particles ending in the photographic emulsion consists of determining pairs of points along the two tracks where the grain density has the same value. At such corresponding points the velocities of the two particles are the same and therefore the residual ranges are proportional to the respective masses. In practice, however, it has been found preferable to plot (usually on a double logarithmic scale) the total number,  $N$ , of grains from a given point to the end of the track vs. the residual range,  $R$ . Since the grain density,  $dN/dR$ , and also the ratio  $R/m$ , are functions of the velocity alone, one can write:

$$\frac{dN}{dR} = f\left(\frac{R}{m}\right), \quad (1)$$

where  $f$  is the same function for particles of all masses.

From this equation it follows that:

$$N(R) = mF\left(\frac{R}{m}\right), \quad (2)$$

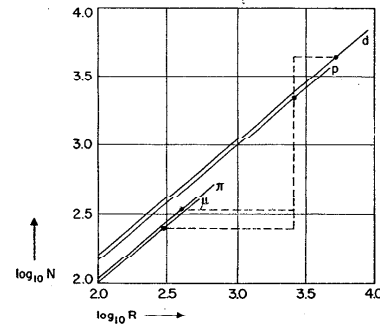


Fig. 3.16.1. Total number of grains,  $N$ , vs. residual range,  $R$ , in Ilford C2 emulsions for protons ( $p$ ),  $\pi$ -mesons ( $\pi$ ),  $\mu$ -mesons ( $\mu$ ), and deuterons ( $d$ ). The proton curve is obtained from experimental data of Lattes *et al.* (LCM47.2); the other curves are derived from proton curve by means of the theoretical relation (3.16.2).  $R$  is measured in microns.

where  $F$  is also a universal function of  $K/m$ . One can formulate the law expressed by Eq. (2) by saying that the quantity  $(\log N - \log m)$  is a universal function of  $(\log R - \log m)$ . In other words, the curves giving  $\log N$  vs.  $\log R$  for two singly charged particles of masses  $m_1$  and  $m_2$  are identical in shape and are obtained one from the other by a translation of magnitude  $\log(m_1/m_2)$  in both coordinates. As an illustration, Fig. 1 shows the experimental curve of  $\log N$  vs.  $\log R$  for protons (mass  $M_p = 1836m_e$ ) obtained by Lattes and his collaborators (LCM47.2) in Ilford C2 emulsions, along with the curves for particles of mass  $209m_e$  ( $\mu$ -mesons),  $276m_e$  ( $\pi$ -mesons) and  $3673m_e$  (deuterons) obtained from the proton curve by the method outlined above.

(b) *Mass Determinations of Singly Charged Particles from Range and Scattering.* This method has the advantage of yielding an absolute estimate for the mass of a particle that comes to rest in the emulsion. It is, however, subject to large statistical errors unless the track is very long. For an actual mass determination one may proceed as follows: sub-divide the track into a number of equal segments of length  $d$ ; measure the angles,  $\theta_s$ , between the median lines drawn through alternate segments as outlined in the preceding section, and determine the corresponding residual ranges,  $R$ .

For particles of sub-relativistic velocities, Eq. (3.15.4) may be rewritten as follows:

$$|\theta_s E|_{\text{av}} = C\sqrt{d},$$

where  $E$  is the kinetic energy and  $C$  is a constant characteristic of the emulsion. On the other hand, the energy-range relation, Eq. (3.15.2), may be put in the form:

$$E = BR^n m^{1-n},$$

where  $B$  and  $n$  are constants. By combining the two above equations one obtains the following relation:

$$Bm^{1-n} |\theta_s R|_{\text{av}} = C\sqrt{d},$$

from which one can compute  $m$ .

(c) *Mass Determinations of Singly Charged Particles from Grain Density and Scattering.* When a singly charged particle traverses the emulsion without stopping in it, one can still roughly estimate its mass by measuring grain density and scattering. Such an estimate is possible only if the track in the emulsion is sufficiently long (of the order of several thousand microns) and if the momentum of the particle is not too great (less than about 1 Bev/c). This method has proved useful in identifying ionizing particles from nuclear stars.

(d) *Identification of Multiply Charged Particles.* One can identify alpha particles stopping in the emulsion by measuring range and grain density. For example, an  $\alpha$ -particle and a proton with the same residual range have approximately the same velocity (see § 3.15). Therefore, at

equal distances from the end of the track the energy loss of the  $\alpha$ -particle is approximately four times greater than that of the proton.

The tracks of heavier nuclei near the ends of their ranges are unmistakably identified by the great density, the large width and the abundance of  $\delta$ -rays (see Fig. 3.15.1f). A characteristic feature that one will notice on the tracks of heavy nuclei ending in the emulsion is the gradual tapering in the last 100 microns or so. This is due to the fact, already mentioned in the preceding section, that the probability that the nucleus may capture one or more electrons increases as the velocity of the nucleus decreases. The capture probability becomes appreciable when the velocity is of the order of the velocity of electrons in atomic orbits. Below this velocity the effective charge of the nucleus is appreciably smaller than its actual charge,  $ze$ , and tends to zero as the velocity approaches thermal velocities.

When a multiply charged particle ends in the emulsion, one may determine approximately its charge by measuring the numbers of  $\delta$ -rays per unit length at different points of the track and plotting these numbers against residual range. On the same graph one also draws the theoretical

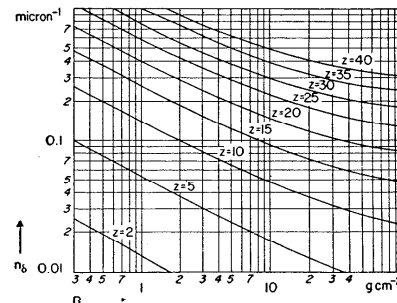


Fig. 3.16.2. Determination of  $z$  from measurements of  $\delta$ -ray density,  $n_\delta$ , and range,  $R$ . The curves are computed from Eq. (3.15.7) and from the range-energy relation for aluminum. The absolute values of the ordinates are obtained from a calibration with  $\alpha$ -particles. From Bradt and Peters (BHL48).

curves, such as those shown in Fig. 2, giving the density of  $\delta$ -rays as a function of range (these curves are obtained from Eq. (3.15.7) and from the energy-range relation). One can then decide which of the theoretical curves fits the experimental data best (see BHL48; SSO49). The experimental uncertainty of the measurements made by this method is usually of the order of 2 units in  $Z$ . As explained in § 3.15, it is necessary to calibrate the emulsion with tracks of known particles in order to determine the scale for the ordinates of the theoretical curves.

In drawing the theoretical curves, one postulates that the probability of detection of a  $\delta$ -ray track is independent of the number per unit length of these tracks (§ 3.15). This may not be rigorously correct. In fact, the experimental data seem to indicate that the probability of detecting a  $\delta$  ray decreases slightly as the density of  $\delta$ -rays increases.

When a multiply charged particle does not stop in the emulsion, one can obtain a lower limit for its charge from the  $\delta$ -ray density by assuming that the particle has relativistic velocity. Sometimes the subsequent interactions of the particle or other criteria prove that the particle actually has relativistic velocity, and the  $\delta$ -ray density then yields the actual value of the mass.

Measurements of the "thin down" length and counting of the "gaps" along the tracks of multiply charged nuclei also can be used to obtain a crude estimate of the charge.

Lastly, we may mention that grain-counting in underdeveloped emulsions seems to offer a promising approach for the identification of nuclei heavier than  $\alpha$ -particles.

**3.17. Scintillation counters.** The scintillation method is one of the earliest tools of nuclear research.\* Practically abandoned for many years in favor of electric counting devices, it was revived in 1947 by the work of Broser and Kallmann (BI47; BI48). In its modern version, a scintillation counter consists of a fluorescent substance, i.e., a substance capable of emitting light when traversed by an ionizing particle, and a *photomultiplier*, that transforms the light pulse into an electric pulse. The electric pulse may be recorded electronically, or it may be presented on the screen of a cathode-ray tube. By operating the photomultiplier at a voltage about 50 per cent higher than the rated voltage, one can obtain from the photomultiplier a pulse of sufficient size to deflect the oscilloscope beam directly. Alternately, one may operate the photomultiplier at the rated voltage and use an electronic amplifier between the photomultiplier and the oscilloscope.

The time dependence of light emission from a fluorescent substance appears to follow an exponential law of the type

$$n(t) = \text{const} \cdot (1 - e^{-t/\tau}) \quad (1)$$

where  $n(t)$  represents the total number of photons emitted during a time  $t$  after the passage of the particle. An expression of the same type of Eq. (1) gives the voltage pulse developed by the photomultiplier, provided the time constant of its output circuit is large compared with  $\tau$  (see § 3.3). Figure 1 shows the oscilloscope record of a pulse from a stilbene crystal. The general shape of this pulse is of the type described by Eq. (1). The

\* See, for example, E. Rutherford, J. Chadwick, and C. D. Ellis, *Radiation from Radioactive Substances*, Macmillan Co., New York (1930), Chapter 2.

step-like discontinuities correspond to the emission of single photo-electrons from the cathode of the photomultiplier.

At room temperature, photomultipliers give many spurious pulses of size comparable with the size of the pulses produced by the light flashes that one wishes to record. To a large extent, one can eliminate these spurious pulses by keeping the photomultiplier at low temperature (with dry ice or liquid air). Alternately, one may use two photomultipliers looking at the same scintillator and record only their coincident pulses. Because of the random and independent distribution of the spurious pulses in the two photomultipliers, the number of coincident spurious pulses is a small fraction of the total number of these pulses in each tube (see § 3.7).



Fig. 3.17.1. Oscilloscope record of the pulse from a stilbene crystal. From W. Kraushaar (unpublished).


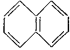
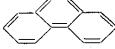
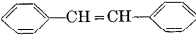
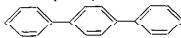
One can manufacture scintillation counters with many different fluorescent substances, some of which are listed in Table 1. These include organic crystals (BI47; BI48), inorganic crystals (HR49), solutions (RGT50; KH50.1), and plastics (SMG50). In order to be useful as a scintillator, a substance must transform a large fraction of the energy received from an ionizing particle into light and must be transparent to its own fluorescent radiation. Also, the emission of light must take place in a short time interval; i.e.,  $\tau$  in Eq. (1) must be small. In this connection, one should note that the decay time of the fluorescent light appears to be an *increasing* function of the temperature of the sample, at least in the case of several organic scintillators (PRF50).

In many cases, and especially for cosmic-ray experiments, it is important that the fluorescent substance should be available in clear samples of fairly large size. In this respect, of course, liquid or plastic scintillators are greatly superior to crystals.

The fluorescence of an inorganic crystal seems to be a property of the crystal as a whole; it is strongly influenced by the presence of impurities and, as a rule, its period  $\tau$  is comparatively long.\* The fluorescence of organic compounds, on the contrary is a property of the molecules and has, in general, a shorter period. The properties that make certain organic compounds useful as scintillation counters seem to be connected with the presence of chains of alternate double bonds in their molecules. The

\* For a theoretical discussion of the fluorescence of potassium iodide, see ref. (SB50).

**Table 3.17.1. Some of the fluorescent substances used in scintillation counters and their main properties.** The decay time of the fluorescent radiation,  $\tau$ , is measured at room temperature, unless otherwise stated. Since the fluorescent lights of different substances have different spectral composition, the measured light yields depend on the type of photomultiplier used.

SUBSTANCE	Chemical Formula	Approximate Relative Light Yield (for $\beta$ -particles)	$\tau$ ( $10^{-8}$ sec)
Sodium iodide (with thallium impurities)	NaI	2*	25 (HR49)
Potassium iodide	KI	0.5*	>100*
Anthracene	$C_{14}H_{10}$ 	1	1.3-3 (CGB48) 3.4 (HR50) 2.1 (MO50) 2.4 (LnA50) 2.3 (PRF50) 1.0 (at $-196^\circ\text{C}$ ) (PRF50)
Naphthalene	$C_{10}H_8$ 	0.25*	5.7 (CGB48) 6.0 (LnA50)
Phenanthrene	$C_{14}H_{10}$ 	0.3*	0.9 (CGB48) 1.0 (MO50)
Stilbene	$C_6H_5CH=CHC_6H_5$ 	0.6* (HR50)	1.2 (HR50) 0.57 (LnA50) 0.85 (MO50)
Terphenyl (dissolved in benzene, tol- uene, or xylene; 3 to 5 g to the liter).	$(C_6H_5)_3C_6H_4$ 	0.28-0.46 (KH50.2)	-0.6**
Solid solution of terphenyl in pol- ystyrene		$\leq 0.6$ (SMG50)	<5 (SMG50)

\* From *Nucleonics*, 6, No. 5, p. 68.

\*\* From G. S. Janes (M.I.T.), unpublished results.

energy spent by an ionizing particle passing through the scintillator goes into excitation of molecular levels and a large fraction of the excitation energy is then transformed into light in transitions leading to levels above the

ground level. Much of the emitted light has a wave length greater than the resonance radiation and therefore is not absorbed by the scintillator. Kallmann and Furst (KH50.2) have discussed in detail the mechanism of light emission from dilute solutions and have concluded that the high light yield of these solutions can be traced to a transport of excitation energy from the solvent to the solute.

Some of the fluorescent inorganic crystals (like NaI) appear to give light pulses proportional to the energy dissipated in the crystal and independent of the spatial concentration of the ionization. For the organic scintillators, instead, the light yield per unit energy dissipation is a decreasing function of the specific ionization (FW50).

To use scintillation counters for quantitative determinations of energy losses, one must, of course, note that the light received by the photomultiplier may depend strongly on the place where the particle has traversed the crystal with respect to the position of the photomultiplier. In addition, one must consider that the electric pulses of a photomultiplier recording light flashes of a given size exhibit fluctuations, because the number of photoelectrons released by each light flash from the cathode is usually small and because the process of multiplication by secondary emission has a statistical character.